CHAPTER 4

Basins due to flexure

Every valley shall be exalted, and every mountain and hill shall be made low: and the crooked shall be made straight, and the rough places plain.

(ISAIAH 40:4)

SUMMARY

Flexure is the long wavelength deflection of a lithosphere of finite strength caused by the application of an external force system. A general flexural equation can be established for the case of a thin elastic plate overlying a weak fluid subjected to vertical applied forces, horizontal forces, and torques or bending moments. The general flexural equation can then be used in different geodynamic situations by applying different boundary conditions.

Flexure of the lithosphere is most clearly demonstrated at oceanic islands, seamount chains, ocean trenches, and foreland basins. Lithospheric flexure also supports sediment loads in most sedimentary basins. The characteristic signature of lithospheric flexure is a negative free air gravity anomaly (at sea) or a negative Bouguer anomaly (on land). The flexural basins associated with ocean–continent and continent–continent plate margins are particularly well represented in the geological record. In an Andean-type setting the flexural basin on the subducting oceanic plate is the ocean trench and the flexural basin on the upper plate is a retroarc foreland basin. In Alpine-type settings the flexural basin on the subducting plate or lower plate is called a peripheral- or pro-foreland basin, whereas the flexural basin on the overriding or indenting plate is termed a retro-foreland basin. Some foreland basins are related to subduction zone roll-back (subduction zone retreat) and are associated with prominent backarc extension. The formation and evolution of foreland basins is intimately related to the processes of shortening, exhumation, and extensional collapse in the adjacent orogenic wedge.

The deflection of the oceanic lithosphere along seamount chains such as the Hawaiian Islands can be explained by either the flexure of a continuous plate loaded by a vertical applied force (representing the excess mass of the seamount chain), or by the flexure of a plate broken beneath the vertical applied force. Some useful and simple expressions for the geometry of the deflection can be derived that involve the maximum amplitude of the deflection, the width of the basin, the location of the forebulge, and the height of the forebulge. In particular, the wavelength of the deflection is dependent on the *flexural rigidity* of the plate, or *flexural parameter*. The maximum deflection is dependent on the flexural rigidity and the magnitude of the applied load.

The bending of the ocean lithosphere at trench–arc systems can be explained by the flexure of a broken elastic plate by a combination of vertical and horizontal forces and bending moments. These forces cannot, however, be directly determined. Forebulges (or outer rises) are very well developed seaward of deep trenches in the northwestern Pacific.

Many studies of continental flexure have been made in collisional zones. Bouguer gravity anomaly profiles across mountain belts and foreland basins suggest a great variability in the make-up of the force systems deflecting the continental plate. This is primarily because of the complexity of crustal and mantle wedging and slab dynamics within and beneath collision zones. Although line load configurations provide reasonable deflections of the continental lithosphere, orogenic wedge loads, and sedimentary basin-fills need to be treated as spatially distributed loads.

There has been much debate about the flexural rigidity of the oceanic and continental lithosphere. The oceanic lithosphere appears to become stronger as it ages and cools, but it does not weaken in its ability to support loads with time since loading. This suggests that any

viscous relaxation that takes place, does so very quickly (less than 10^5 or 10^6 years), after which flexural rigidity approaches an asymptotic value. The factors determining the flexural rigidity of the continental lithosphere are less clear, and there is no relationship between flexural rigidity and its age. A number of factors may be responsible, such as differences in geothermal gradient caused by strong variations in the crustal radiogenic heat production, decoupling between a strong upper crust and strong underlying mantle lithosphere during bending, plastic yielding at high curvatures, and viscoelastic relaxation. The lithosphere approaching collision zones may also be segmented, producing a stepped, compartmentalized deflection. Strong spatial variations in flexural rigidity have been measured in the forelands of many mountain belts.

Although linear elasticity suggests that lithospheric buckling should not take place, analogue experiments and numerical models using more realistic lithospheric rheologies consistently reproduce long wavelength (several hundred km) antiforms and synforms. The topography of basins in, for example, central Asia, supports the existence of lithospheric buckles. Sedimentary basins located at buckle synforms may be difficult to discriminate from backbulge depositional zones.

Orogenic wedges act as primarily vertical loads on the deflected plate in collision zones. The movement of a line load or distributed load over a foreland plate forces a wave-like deflection ahead of it. The orogenic wedge is viewed as a dynamic unit with critical surface slopes in which the gravitational and deviatoric forces strive to achieve a steady state. Disturbances of equilibrium by externally imposed forces (such as changes in convergence rate) may result in major changes in the rates of shortening or extension of the wedge. These processes in turn influence the erosion of the mountain belt to provide detritus for the foreland basin and the configuration of the load causing the deflection of the overridden plate. Critical taper models modified to allow for brittle–ductile behavior suggest that the topographic profiles of some mountain belts, such as the Andes, can be explained by the changing ratio of basal shear stress in the decollement zone and strength of rocks in the lower part of the wedge. Ductile behavior in the hotter part of the wedge and within the deep basal shear zone cause a shallow foothills region, steeper intermediate segment, and elevated plateau physiography.

Analogue models using scaled physical experiments are successful at visualizing major crustal structures produced during convergence, including major crustal buckles, conjugate shears, and bivergent wedges. Early numerical models focused on diagnostic basin stratigraphy, treated erosion, sediment transport and deposition as a diffusional problem. Later 3-D plane strain numerical models illustrate the complex links between plate convergence, tectonic fluxes within bivergent wedges, and exhumation. The mechanics of these wedges can be investigated using the Argand number and Ampferer number. Two dynamical end members are the indentation model and the subduction model. Plane strain numerical models show that erosion of the surface of the orogenic wedge is of major importance to wedge dynamics as well as to the filling of adjacent foreland basins. Such models now provide a mechanical explanation for the topography, distribution of high grade metamorphic rocks and thermochronology of rocks in orogenic belts.

In Chapter 4 we focus on the process of lithospheric flexure with the goal of better understanding the behavior of the lithosphere when acted upon by applied force systems or loads. This is of relevance in a number of situations in basin analysis. First, flexure of the lithosphere may cause the primary subsidence or uplift in a sedimentary basin. The most important example is the downflexing of a continental plate by force systems set up during mountain building. This produces *foreland basins*. Second, the lithosphere may undergo a long wavelength flexure in supporting sediment loads. This takes place in basins of all types, including those due to stretching of the lithosphere (Chapter 3).

Foreland basins are elongate or arcuate, highly asymmetrical basins closely associated with continental collision zones. The alternative term "foredeep" was introduced by Price (1973). Dickinson (1974) proposed two genetic classes of foreland basin (Fig. 4.1): (i) Peripheral foreland basins situated against the outer arc of the orogen during continent–continent collision (e.g., Indo–Gangetic Plain, north Alpine foreland basin). (2) Retroarc foreland basins situated behind a magmatic arc linked with subduction of oceanic lithosphere (e.g., Andean examples, Late Mesozoic–Cenozoic Rocky Mountain Basins, North America). Both classes of foreland basin overlie cratonic lithosphere and are associated with crustal shortening in tectonically active zones. Some highly arcuate thrust belts and spatially restricted foreland basins are related to *subduction zone roll-back* and are commonly associated with important backarc extension (Fig. 4.1). The Apennines–Tyrrhenian Sea of the western Mediterranean is an example.

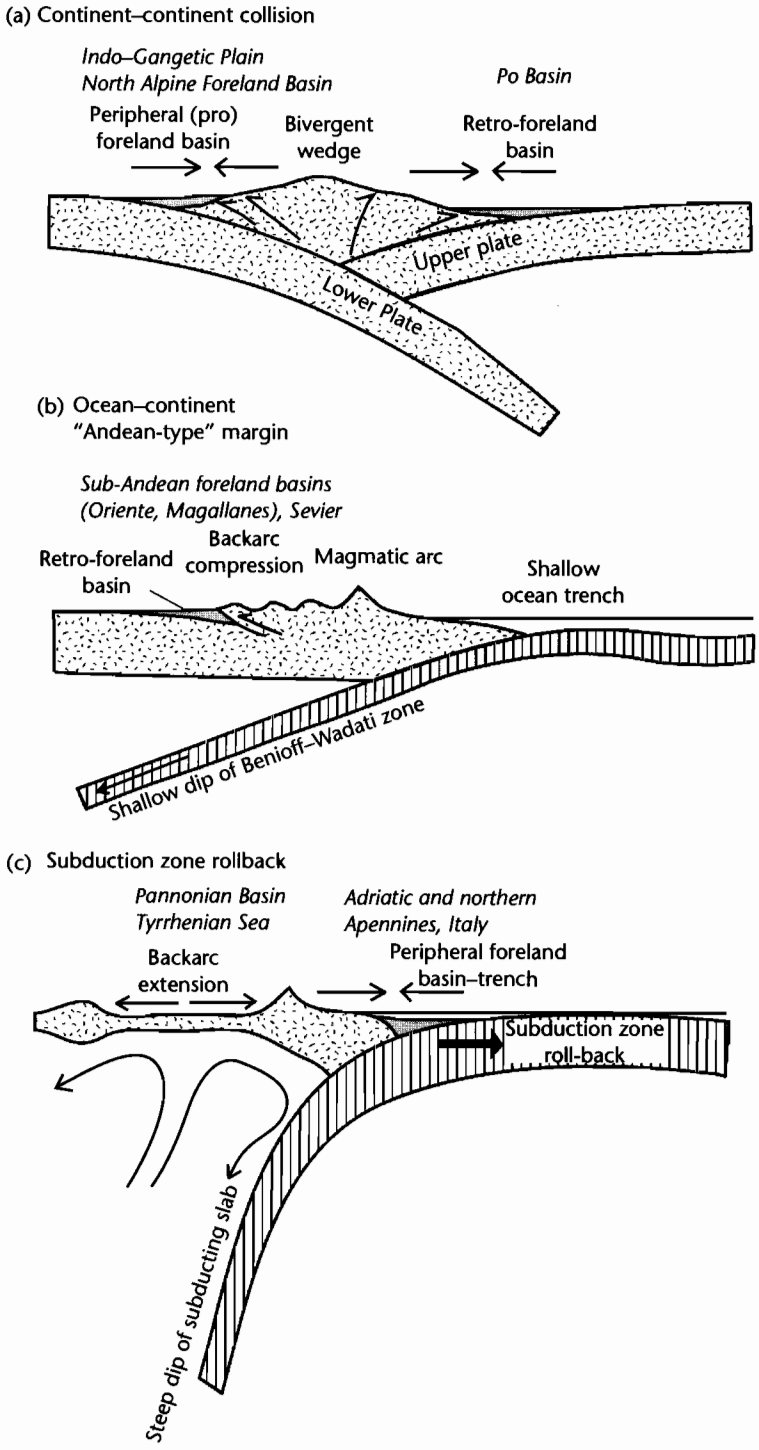

Fig. 4.1 Schematic illustration of peripheral foreland basins, retro-foreland basins, and basins related to subduction zone roll-back.

A mechanically similar situation to continental collision zones exists at ocean–ocean and ocean–continental collision zones where oceanic lithosphere is subducted. The complex plate boundary zone contains many structurally controlled basins. The mechanical equivalent of the orogenic wedge on continental lithosphere is the accretionary prism, with a forearc basin on its retro-flank, and an oceanic trench on its pro-flank.

The lithosphere is capable of distributing forces imposed by a load by a horizontal transmission of stresses. A general flexural equation (eqn 2.29) involving vertical applied loads, horizontal pressure forces, and torques or bending moments can be established for the case of a thin linear elastic plate in a state of plane strain, a reasonable approximation for the lithosphere. In the case of foreland basins, continental lithosphere is bent under the sum total of loads imposed by orogenesis. In the case of ocean trenches and forearc basins, the oceanic lithosphere is bent prior to subduction. We shall now examine these cases in more detail in order to investigate the precise nature of the basin-forming forces.

The reader is referred to §2.1.3 and §2.1.4 for some of the fundamentals of flexure of linear elastic materials. §2.4 contains background to more complex rheologies. In this chapter we concentrate on the application of ideas on flexure to the geometry of ocean trenches and particularly foreland basins. §8.3.1 discusses the stratigraphic patterns in basins of this type.

4.1 BASIC OBSERVATIONS IN REGIONS OF LITHOSPHERIC FLEXURE

Both oceanic and continental lithosphere are capable of a long wavelength bending termed flexure. Flexure of the oceanic lithosphere takes place at ocean trenches, mid-ocean ridges, seamount chains and individual oceanic volcanic islands. Flexure of the continental lithosphere takes place at sites of rifting, strike–slip faulting, at passive margins, and most emphatically at sites of plate convergence. The sedimentary basins caused by flexure of continental lithosphere located adjacent to zones of tectonic shortening commonly occur as pairs, separated by an orogenic belt or magmatic arc (Fig. 4.1). Flexural basins are elongated along the tectonic strike, with an asymmetrical cross-section deepening towards the orogenic belt or magmatic arc. On the continental lithosphere, Bouguer gravity anomalies are negative, indicating the presence of a mass deficit at depth, caused by the downward penetration of relatively light "granitic" material, replacing mantle. Flexural basins on continental lithosphere are close to strongly eroding source areas, and are typically filled with large thicknesses of synorogenic sediment. Ocean trenches, however, may be well-nourished or starved of sediment depending on the proximity of major sediment routing systems. Heat flows in regions of lithospheric flexure are close to normal, or slightly reduced due to crustal and lithospheric thickening during plate convergence.

In the following sections we separately consider some of the basic observations supporting flexure at ocean trenches and foreland basins.

4.1.1 Ocean trenches

At ocean–ocean and ocean–continent convergent boundaries, there is strong evidence that the oceanic lithosphere is bent to high curvatures. Seaward of the ocean trench is a positive free-air gravity anomaly (Watts and Talwani 1974) which corresponds to relatively elevated seafloor. The trench and accretionary prism are characterized by a large negative free-air gravity anomaly, and the island arc by a large positive anomaly (Fig. 4.2). These anomalies can be explained by the bending of the oceanic plate by an applied force system. The shape of the plate at depth can be imaged from the foci of the earthquakes that define Benioff–Wadati zones (Fig. 1.7). First motion studies of these earthquakes show different solutions according to location in the downgoing slab. On the outer wall of the trench the earthquakes are tensional and located down to 25 km depth. This is thought to be a response to outer arc bending stresses in the highly curved oceanic lithosphere. The contact between the upper surface of the downgoing plate and the overriding plate is marked by reverse fault focal mechanism solutions, due to the frictional contact and compressive deformation between the two plates. At much greater depths earthquakes occur at 30–40 km below the top of the slab, suggesting that they occur as the result of internal deformation of the downgoing plate, rather than as a result of compression against the opposite plate. The focal mechanism solutions suggest that the descending plate at these depths is in a state of either down-dip compression or extension (Isacks et al. 1969; Isacks and Molnar 1971), depending perhaps on the net effect of slab pull and ridge push forces on the plate (Spence 1987).

The ocean trenches of the world are remarkably uniform in their bathymetry and wavelength (Fig. 4.3). They are generally 50–100 km in width and 2–4 km below the general level of the adjacent ocean floor. They are asymmetrical in cross-section with a steeper limb

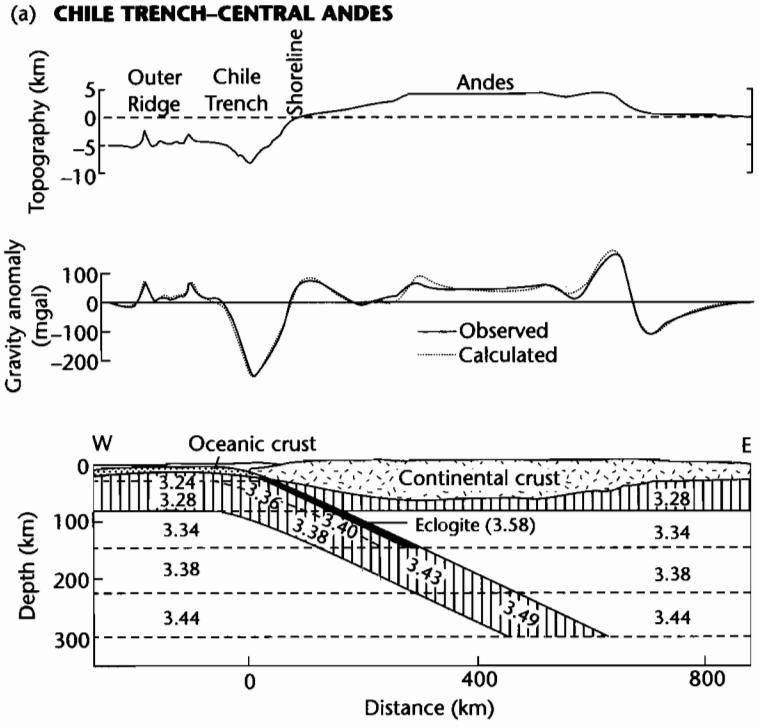

Fig. 4.2 Cross-sections of the arc–trench systems of the Andes and northwestern Pacific. (a) Topography, free-air gravity anomaly, and density model for a cross-section of the Chile Trench and central Andes at 23 °S, after Grow and Bowin (1975). Reproduced courtesy of American Geophysical Union; (b) Topography, free-air gravity anomaly, and crustal density model for the Japan Trench and arc, after Yoshii (1979), Matsuzawa et al. (1986), and van den Beukel and Wortel (1986). Reproduced courtesy of Cambridge University Press.

flanking the overriding plate, and a shallow slope on the side of the downgoing plate. Most trenches are relatively starved of sediment (e.g., Tonga), whereas others are filled with sediment (e.g., Lesser Antilles, and northern part of Burmese–Sunda Trench) and therefore lack a pronounced bathymetric expression. The key control is the availability of a major source of sediment; for example, the Ganges–Brahmaputra and Irrawaddy systems are responsible for the filling of the Burma Trench, while the same trench in Sumatra is relatively deficient in sediment fill.

Cross-sections of the Andes indicate that where the dip of the downgoing slab is shallow, as in Ecuador, there is very little volcanism and weak but widespread seismicity (Pilger 1984). Deformation extends from the active plate margin huge distances (up to 700 km) into the center of the plate, giving rise to crustal shortening and earthquake activity in fold–thrust belts facing the craton. Where the plate is being subducted at a high angle, there is active recent volcanism, seismicity is restricted to a narrow Benioff zone, and a well-developed longitudinal median sedimentary trough (Altiplano) is developed. The cause of the locally shallow angle of the downgoing slab may be the subduction of relatively buoyant oceanic ridges or of very young oceanic lithosphere.

4.1.2 Foreland basins

There are also elongate to arcuate basins located at ocean–continent and continent–continent collision zones (Fig. 4.1) where they are situated on continental lithosphere (Dickinson 1974). In an Andean-type setting (ocean–continent), the basin on the lower plate is the ocean trench, and the basin on the upper plate is a foreland basin, commonly termed of *retroarc type*. In a

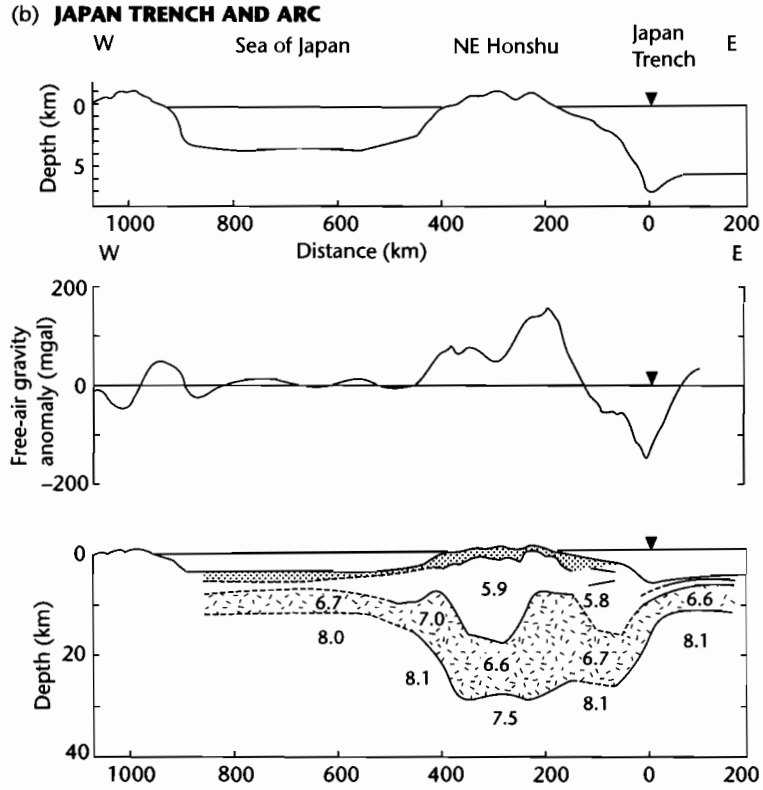

Fig. 4.2 *Continued*

Himalayan-type or Alpine-type setting (continent–continent), the foreland basin on the lower plate is of *peripheral* or *pro-foreland* type, and the basin on the upper plate is of *retro-foreland* type (Willett et al. 1993). Some orogenic belts contain large *intramontane basins*, as is classically displayed in the Andes of South America (Horton et al. 2001). However, these intramontane basins are caused by localized extensional and strike–slip tectonics rather than lithospheric flexure. Foreland basins may be partitioned by the uplift of crustal blocks cored by basement rocks (Schwartz and DeCelles 1988), as in the Laramide uplifts of the Rocky Mountains of the western interior of USA.

Foreland basin systems are dynamically linked to adjacent convergent orogenic belts. These convergent orogens are zones of considerable (hundreds of km) crustal shortening, achieved by translations along thrust faults and by ductile thickening. The thrust belts characteristic of orogenic belts are typically parallel to the strike of the orogenic belt, but in detail comprise salients and reentrants (syntaxes). The Appalachians of eastern North America and the Himalayas of India–Pakistan are Paleozoic and Cenozoic examples respectively. Many orogenic belts are also characterized by ductile extensional detachment faults and shear zones that facilitate rapid rates of exhumation of high grade rocks. The South Tibet Detachment System of the Himalayas (Burg et al. 1984) and the Simplon Fault of the Swiss Alps (Mancktelow 1985) are examples.

Some thrust belts and foreland basins are related to *subduction zone roll-back*, or *subduction zone retreat* (Royden 1993), where the rate of subduction exceeds the rate of plate convergence. Subduction roll-back produces short, highly arcuate thrust systems such as the Apennines and Carpathians of Europe. Foreland basins developed in such systems may be associated with regions of retroarc extension (e.g., Pannonian Basin) or the creation of new oceanic basins (Apennines–Tyrrhenian Sea, Malinverno and Ryan 1986; Doglioni et al. 1998).

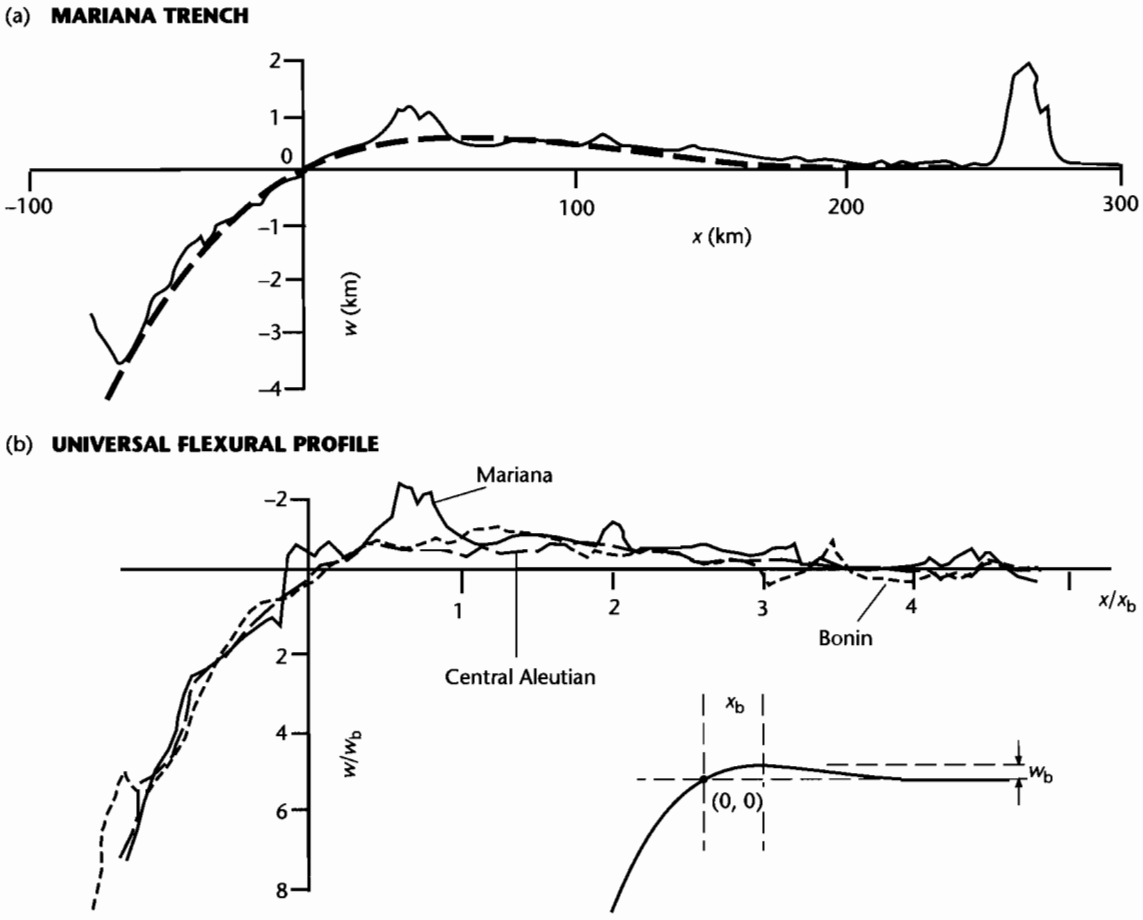

Fig. 4.3 (a) Bathymetry of the Mariana Trench (Watts and Talwani 1974) compared to that predicted by the universal flexural equation with x_b taken as 55 km, and w_b as 0.5 km (after Turcotte and Schubert 1982, p. 130); (b) Nondimensional comparison of the bathymetric profile of the Mariana, Bonin, and Central Aleutian oceanic trenches with a universal flexural profile (after Caldwell et al. 1976). The bathymetric profiles are normalized as described in §4.2.3. Reproduced courtesy of Cambridge University Press.

There are a number of well-documented orogenic belts and foreland basin systems related to Cenozoic orogenesis, such as the Pyrenees of Spain, Alps of France and Switzerland, Apennines of northern Italy, Himalayas of India and Pakistan, and Andes of South America. These examples provide benchmarks of the close linkage between lithospheric flexure, convergent tectonics, and basin development. As an example, the Himalayas are the world's highest and largest orogenic belt. A classic foreland basin (Burbank et al. 1996) with >6 km of sedimentary fill is found to the south of the Main Boundary Thrust of the Himalayan system (Fig. 4.4). The Himalayas are 250–350 km wide and extend for thousands of kilometers around the site of indentation of India with Asia. Convergence between the Indian indenter and Asia is currently *c.* 60 mm y^{-1} (Bilham et al. 1997). Shortening in the Himalayan fold–thrust belt is in excess of 700 km (DeCelles et al. 1998). Focal mechanism solutions of earthquakes (Molnar and Chen 1982) show that the Indian shield in the south is undergoing weak extensional faulting, the Lower Himalaya is experiencing thrust fault deformation, and the High Himalaya has a mixture of extensional and strike–slip deformation. Seismic imaging shows that

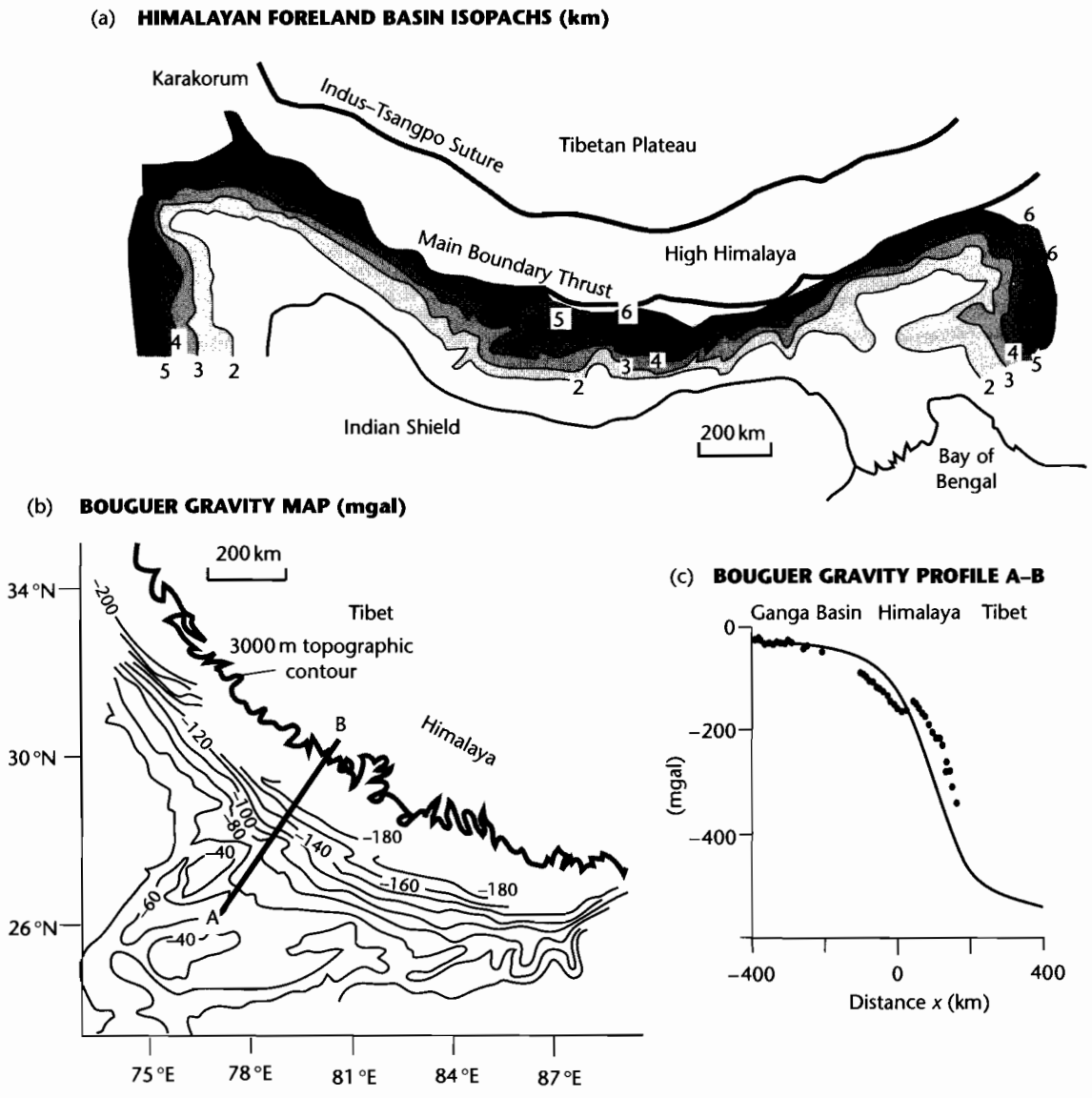

Fig. 4.4 The Himalaya and Ganga Basin. (a) Isopach map of sediment thicknesses in the Himalayan foreland basin, based on Raiverman et al. (1983); (b) Contours of Bouguer gravity anomaly over the Ganga Basin, and (c) observed Bouguer gravity anomalies along profile A–B, compared with the anomalies computed assuming the topography is locally compensated (Airy model) by thickening of the crust beneath central India. Note that there is an apparent mass excess in the Himalaya and a mass deficit over the Ganga Basin (after Lyon-Caen and Molnar 1985).

the Moho descends from about 35 km under the Indian shield, *via* a number of steps, to 70 km under Tibet. Although it is unlikely that the Indian plate slides smoothly under Asia, the gravity data in the Ganga Basin and Himalaya (Lyon-Caen and Molnar 1985) can be explained by the flexure of the Indian plate beneath the topographic load of the mountain belt (Fig. 4.4).

Foreland basins are therefore emphatically syn-orogenic. The bulk of the sediments in foreland basin systems (DeCelles and Giles 1996) are found in a *foredeep*, extending from the thrust front across the foreland plate (see also §8.3.1). The foredeep is classically asymmetrical, with subsidence rates at a maximum close to the thrust front. Sedimentation is dominated by sediment delivery from the orogenic belt, but significant sediment discharges may come from the opposite side of the basin, particularly early in basin development. Proximal foredeep deposits are progressively incorporated into the orogenic wedge as the thrust belt migrates over the foreland. Sediments also accumulate in *wedge-top* or *piggy-back basins* located on top of the deforming thrust wedge. These basins are commonly involved in thrust deformation, and may be eroded as the orogenic wedge is exhumed.

4.2 FLEXURE OF THE LITHOSPHERE: GEOMETRY OF THE DEFLECTION

Since the oceanic lithosphere has a relatively simple thermal structure and is relatively simple rheologically, it is the appropriate starting place for the consideration of flexure. Early measurements of free-air gravity anomalies in the ocean were highly influential in explaining the bathymetry of the seafloor, particularly adjacent to oceanic islands and seamount chains. Where there is negligible sediment loading, the bathymetry of the ocean floor and its free-air gravity anomalies can be explained by a model involving a line load acting on either a continuous plate (§4.2.1) or on the end of a broken plate (§4.2.2). The effect of a load system that has a significant spatial distribution is discussed in §4.2.3.

4.2.1 Deflection of a continuous plate under a line load

Some general concepts of flexure can be appreciated by considering the bending of oceanic lithosphere under loads acting a long way from the edge of the plate. A geological situation of this type is the flexure of the lithosphere under the load of mid-plate oceanic islands such as the Hawaiian archipelago (Vening-Meinesz 1941, 1948; Watts and Cochran 1974). The Hawaiian ridge is a long (thousands of km) line of volcanic islands of about 150 km width. The ridge therefore approximates a line load. The ridge is flanked by a depression, the Hawaiian Deep and then an outer rise

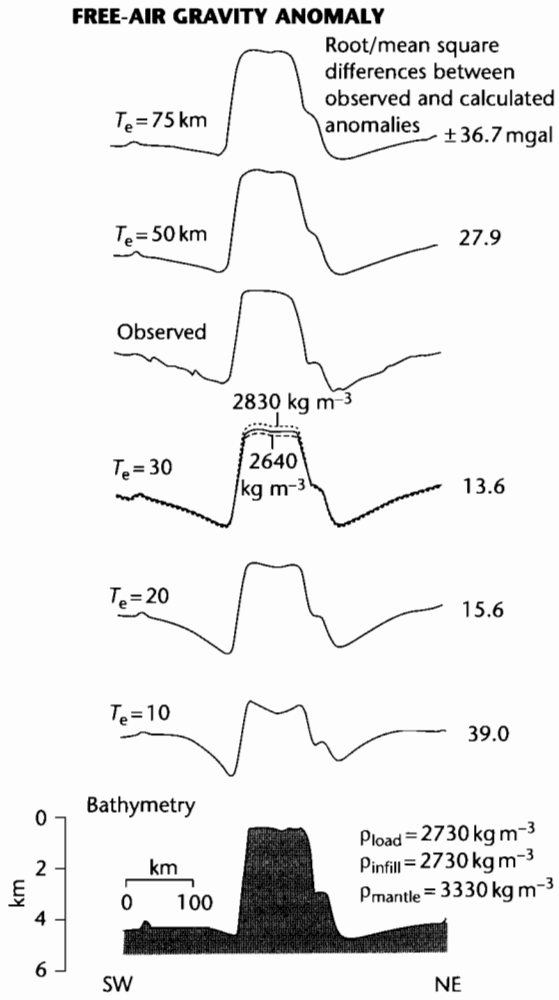

Fig. 4.5 Free-air gravity and bathymetry along a transect that intersects the Hawaiian Islands between Oahu and Molokai (Watts and Cochran 1974; Watts 2001). The seamount chain is associated with a free-air gravity high and the fringing moat by a free-air gravity low. Beyond a lateral distance of about 150 km the free-air anomalies become positive in the outer rise, which gives an indication of the width of the flexural depression. Calculated profiles using an elastic plate model are shown for a range of equivalent elastic thicknesses (10–75 km). The best fit is for a *Te* of 30 km. Reproduced courtesy of Cambridge University Press.

(Fig. 4.5). These three morphological elements (load, basin, and outer rise or forebulge) are a constant theme in flexural problems.

Taking the boundary conditions for the flexural force balance (eqn. 2.29) as follows:

The applied vertical load, $q_a(x) = 0$, except at the location of the Hawaiian ridge ($x = 0$), and

$P = 0$ since no horizontal forces are applied, then

$$D\frac{d^4w}{dx^4} + \Delta\rho g w = 0 \tag{4.1}$$

where w is the deflection, x is the horizontal scale, D is the flexural rigidity, and $\Delta\rho$ in this case is the difference in density between mantle and infilling ocean water.

The general solution for a fourth order differential equation such as this is accomplished by breaking it into exponential, sine and cosine components (it is in the form of damped sinusoids)

$$w = e^{x/\alpha}(C_1 \cos x/\alpha + C_2 \sin x/\alpha) + e^{-x/\alpha}(C_3 \cos x/\alpha + C_4 \sin x/\alpha) \tag{4.2}$$

where the constants C_1, C_2, C_3, and C_4 are determined by the boundary conditions and α is the *flexural parameter* (Walcott 1970), given by

$$\alpha = \left\{\frac{4D}{\Delta\rho g}\right\}^{1/4} \tag{4.3}$$

Following from the determination of the constants for the case of a line load bending the plate symmetrically (see Turcotte and Schubert 2002, pp.124–6), some useful and simple expressions emerge for the geometry of the deflection (Fig. 4.6). If the maximum deflection (w_0 at $x = 0$) is known, the profile of the deflection of the plate obeys

$$w = w_0 e^{-x/\alpha}(\cos x/\alpha + \sin x/\alpha) \tag{4.4}$$

The half-width of the depression (x_0) can be found since it is defined by the horizontal distance from the maximum deflection ($x = 0$) to the point where the deflection is zero ($w = 0$). Setting $w = 0$, equation (4.4) gives

$$x_0 = \frac{3\pi\alpha}{4} \tag{4.5}$$

The distance from the line load ($x = 0$) to the highest part of the forebulge (x_b) can be found since at the forebulge crest, the slope of the deflection is zero. That is, $dw/dx = 0$ at $x = x_b$. Equation (4.4) then gives

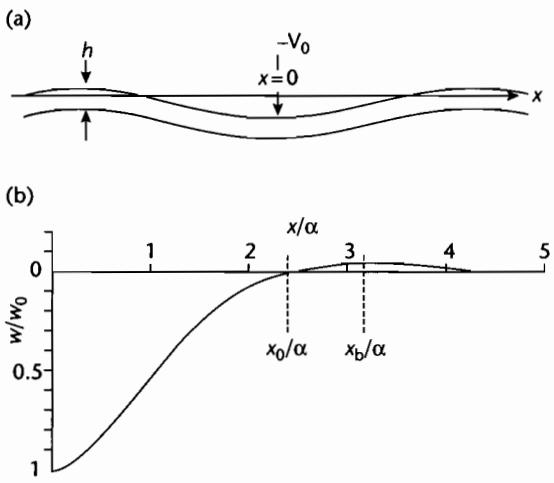

Fig. 4.6 (a) Deflection of a continuous elastic plate under a line load; (b) Theoretical deflection of the elastic lithosphere under a line load applied at the centre of an infinitely extensive plate. Parameters are defined in the text. The deflection w is scaled against the maximum deflection w_0. The horizontal distances are scaled against the flexural parameter α. Bending moments and horizontal in-plane forces are zero.

$$x_b = \pi\alpha \tag{4.6}$$

The height of the forebulge w_b above the datum of zero deflection can also be found using the condition that $x = \pi\alpha$ at the point where $w = w_b$. As a result equation (4.4) reduces to

$$w_b = -w_0 e^{-\pi} = -0.0432 w_0 \tag{4.7}$$

If the deflection under a line load approximates a sedimentary basin, the half width of the basin is represented by x_0 if base level is taken as $y = 0$. However, the half-width enclosed by the deflection is represented by x_b.

By comparison of the observed with the theoretical bathymetric or free-air gravity profiles, something can be said about the thickness of the equivalent elastic lithosphere (defined in §2.1.4) under the Hawaiian islands, always assuming the theory to be an adequate representation of the geodynamics (Watts and Cochran 1974). For example, the bathymetric profile suggests that the crest of the outer rise is about 250 km from the line load of

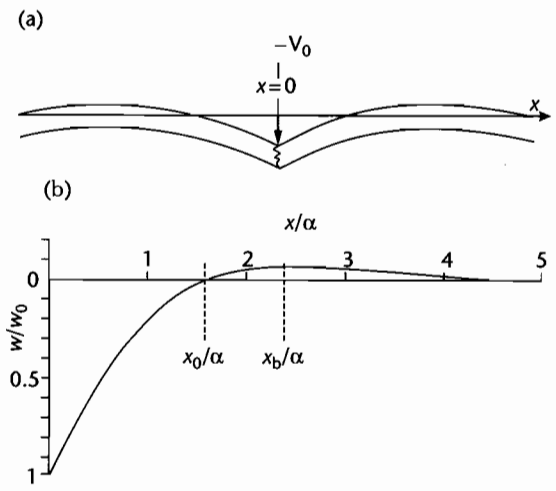

Fig. 4.7 (a) Deflection of a broken elastic plate under a line load applied at its end. Horizontal in-plane forces and applied bending moments are again zero; (b) Theoretical deflection of the broken plate under a line load applied at its end. Note that the half-width of the basin is narrower than for the unbroken plate, and that the elevation of the forebulge is greater than for the unbroken plate. Vertical and horizontal axes are scaled by w_0 and flexural parameter α respectively.

the Hawaiian Islands, i.e., $x_b = 250$ km. Assuming the moat to be water-filled, $\Delta\rho = 2300\,\mathrm{kg\,m^{-3}}$. With a gravitational acceleration of $10\,\mathrm{m\,s^{-2}}$, the flexural parameter from (4.6) is 80 km, which gives from (4.3) a flexural rigidity of 2.4×10^{23} Nm. If Young's modulus E is 70 GPa and Poisson's ratio $\nu = 0.25$, this gives an equivalent elastic thickness of 34 km.

4.2.2 Deflection of a broken plate under a line load

If the Hawaiian plate were broken under the Hawaiian Islands, the boundary conditions of the model of the lithosphere would need to be modified (Walcott 1970). In this case, we would consider the deflection of a semi-infinite elastic plate subjected to a line load $V_0/2$ applied at its end (Fig. 4.7). Assuming that no external torque is applied at $x = 0$, simple expressions describing the geometry of the deflection can be obtained as follows.

The maximum deflection for a broken plate of the same flexural rigidity and under the same vertical load is twice that of an unbroken plate (Turcotte and Schubert 2002, p.126). If the maximum deflection is known, the deflection as a function of x for a broken plate loaded at its end is given by (Turcotte and Schubert 2002, pp.127–9)

$$w = w_0 e^{-x/\alpha} \cos x/\alpha \tag{4.8}$$

The half width of the basin (at $w = 0$) is given by

$$x_0 = \frac{\pi\alpha}{2} \tag{4.9}$$

showing that the basin is narrower for the case of a broken plate. The distance to the crest of the forebulge (where $dw/dx = 0$) is given by

$$x_b = \frac{3\pi\alpha}{4} \tag{4.10}$$

showing that narrower forebulges characterize broken plates. Finally, the height of the forebulge (where $x_b = 3\pi\alpha/4$) is given by

$$w_b = w_0 e^{-3\pi/4} \cos 3\pi/4 = -0.0670 w_0 \tag{4.11}$$

indicating a considerably larger forebulge amplitude for a broken plate.

Returning to the case of the Hawaiian Islands with $x_b = 250$ km (see above), equation (4.10) gives 106 km for the flexural parameter, and flexural rigidity is therefore 7.26×10^{23} Nm. The equivalent elastic thickness with $E = 70$ GPa and $\upsilon = 0.25$ is 49 km.

Seismic refraction studies (Shor and Pollard 1964) suggest that the Moho is deflected downwards by approximately 10 km under the center of the Hawaiian Islands. If 10 km is the maximum deflection w_0, the height of the outer rise above the undeflected seafloor can be found from equation (4.7) for the unbroken plate and equation (4.11) for the broken plate. The results are 432 m and 670 m respectively. Measurements of the bathymetry of the seafloor surrounding the Hawaiian Islands indicate that the outer rise is elevated above regional by about 500 m (Chase et al. 1970) but this does not permit us to tell whether the continuous or broken plate best fits the observational data.

Submarine processes such as erosion or draping with sediment, volcanism and tectonics may cause significant changes to the bathymetric profile. Gravity profiles have

therefore been used to investigate the deflection curve across the Hawaiian area (Fig. 4.5). Free-air gravity anomalies in several profiles across the Hawaii–Emperor seamount chain (Watts and Cochran 1974) show a conspicuous gravity high (<250 mgal) corresponding to the positive bathymetry of the volcanic islands. This is because the free-air gravity anomaly records the excess density of the volcanic edifices relative to seawater. Flanking the central gravity high is a pair of long wavelength gravity lows (<−100 mgal), corresponding to the topographic moat surrounding the seamount chain. Beyond the gravity lows, at a distance of 150–200 km from the line of volcanic islands, are free-air gravity anomaly highs (<50 mgal), once again corresponding to the elevated seafloor of the outer rises.

A good fit was found between the observed free-air gravity anomalies and those calculated for the continuous elastic plate if $D = 5 \times 10^{22}$ Nm, and for the broken elastic plate if $D = 2 \times 10^{23}$ Nm. These values are close to the flexural rigidities estimated from the wavelength of the deflection given above.

Another geological situation is of the bending of oceanic lithosphere at arc–trenches. This configuration is similar to that of an end load on a broken plate, but in this case we cannot ignore the bending moments acting on the subducting plate. Subducting oceanic slabs are subject to a large number of forces. There is a large force acting downwards due to the negative buoyancy of the cold oceanic lithosphere. This may be enhanced at depths of 200–300 km where the olivine to spinel phase change takes place. The oceanic slab also experiences resistance to its downward motion at its tip, which may have a horizontal and rotational (torque) component. It also experiences resistance along its upper contact with the overriding plate, which also has a horizontal component, as has been suggested for the Taranaki–Wanganui region of New Zealand, where the Pacific plate becomes "locked" against the Australian plate (Stern et al. 1992).

Turcotte and Schubert (2002, pp.127–9) give the solution for the deflection by applying the boundary conditions for an ocean trench to the general flexural equation. This solution incorporates the contribution of vertical forces and bending moments to the deflection. Whatever their origin, they cannot be directly determined. However, it is possible to obtain some estimates of the geometrical aspects of the flexural depression by expressing the trench profile in terms of the height of the forebulge (w_b) and the half-width of the forebulge ($x_b - x_0$) (Fig. 4.8). The solution for the latter is

$$x_b - x_0 = \pi\alpha/4 \tag{4.12}$$

In other words, the half-width of the forebulge is a direct measure of the flexural parameter. A forebulge is well developed seaward of deep sea trenches in the northwestern Pacific (Watts and Talwani 1974). The observed bathymetric profile across the Mariana Trench (Fig. 4.3) suggests that the half-width of the forebulge (measured on the flank facing the trench) is about 55 km. Equation (4.12) then gives 70 km for the flexural parameter. Using $E = 70$ GPa, $\nu = 0.25$, and $\Delta\rho = 2300\,\mathrm{kg\,m^{-3}}$, from equation (4.3) the flexural rigidity of the Pacific plate at the Marianas Trench using the broken plate model is 1.35×10^{23} Nm, equivalent to an elastic thickness of 28 km.

Both the deflection w and the height of the forebulge w_b are functions of the flexural parameter and bending moment. Dividing the expression for w by the expression for w_b (i.e., w/w_b) eliminates the unknown parameters and gives a universal flexure profile of the type shown in Fig. 4.8. This universal profile applies to any 2-D elastic flexure under end loading, so can be applied to a variety of geological contexts.

As an example of its application, let us return to the case of oceanic trenches, such as the Mariana, Bonin and Central Aleutian Trenches (Fig. 4.3). For the Mariana Trench, taking horizontal distances from the point $x = 0$ at the oceanward intersection of the plate surface with sea level, the distance to the crest of the forebulge is approximately 55 km and its height is taken as 0.5 km (Fig. 4.3a). The three trenches are shown in terms of dimensionless depth versus dimensional horizontal distance in Fig 4.3b. Although the fit between the theoretical deflection and the observed bathymetry is not perfect, particularly where volcanoes have built cones in the forebulge region, the correspondence is generally good, suggesting that the lithosphere at ocean trenches can indeed be modeled in this way.

The flexure of a semi-infinite elastic oceanic plate at trenches was studied by Watts and Talwani (1974). Although the bathymetry of the Mariana Trench could be explained by purely a vertically applied force at the end of the plate, the Aleutian and Kuril Trenches were better explained by a model involving both a vertical applied force (V) and a horizontal applied force (P, where $P = 5\,V$). However, a bending moment at the end of the plate would reduce the necessity of a horizontal force to explain the deflection (Hanks 1971).

The same approach can initially be taken to the flexure of the continental lithosphere. As in the case of the

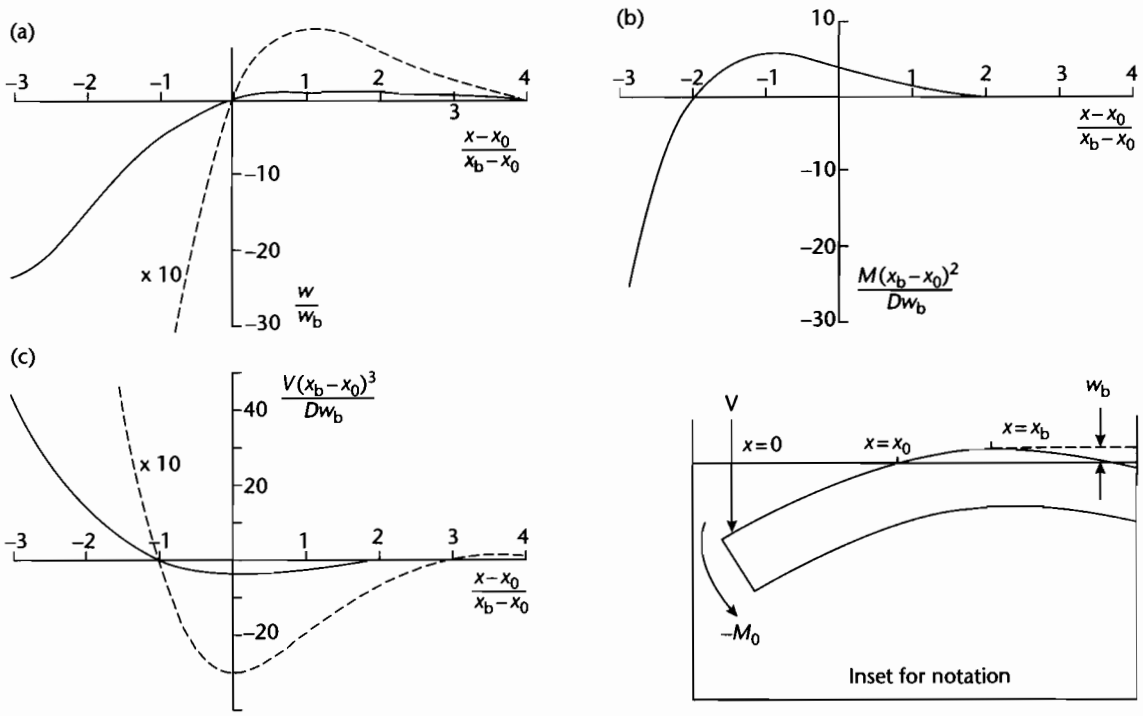

Fig. 4.8 Universal solution for the deflection of an elastic lithosphere under a vertical end load and a bending moment, approximating to the situation at ocean trenches. (a) Dependence of the nondimensional displacement w/w_b on the nondimensional position $(x-x_0)/(x_b-x_0)$. Dashed line shows vertical exaggeration of 10:1 to show geometry of forebulge; (b) The nondimensional bending moment $(M(x_b-x_0)^2/Dw_b)$ versus nondimensional position. Note that the maximum bending moment is found roughly one-third of the distance from $x=x_0$ to the maximum deflection; (c) The nondimensional vertical shear force $(V(x_b-x_0)^3/Dw_b)$ as a function of nondimensional position, showing that it reaches a maximum at the point of maximum deflection. Dashed line is at vertical exaggeration of 10:1. Inset shows notation.

oceanic lithosphere, the universal flexural profile of Figure 4.8 should be applicable, but since regions of continental collision are characterized by mountains acting as source areas for large volumes of detritus, basins occupying the flexural depressions tend to be rapidly filled with sediment. As a result $\Delta\rho$ in the flexural parameter (eqn 4.3) is the difference between mantle and sediment densities, $\rho_m - \rho_s$.

As in the case of the Mariana Trench, it is possible to match a theoretical deflection to the observed depth of basement in a region of continental flexure such as the Appalachians (Fig. 4.9). The best fit of the theoretical curve to the basement shape is by choosing $x_b - x_0 =$ 122 km (half-width of forebulge) and $w_b = 0.29$ km (height of forebulge). As must be obvious when considering a Paleozoic foreland basin, much information has been lost through erosion and the choice of parameters above is therefore neither unique nor verifiable. The close match between theory and observation in Fig. 4.9 merely gives some confidence in treating the geodynamic problem as essentially one of flexure. The flexural rigidity implied by the Appalachian profile in Fig. 4.9 is 10^{24} Nm (equivalent elastic thickness of 54 km). This suggests that the flexural rigidity of continental lithosphere can be greater than that of oceanic lithosphere.

4.2.3 Deflection of a continuous plate under a distributed load

Flexural basins on the continental lithosphere, such as foreland basins, are generally loaded by a force system that has a spatial distribution far removed from a line-load approximation. Consequently, it is necessary to con-

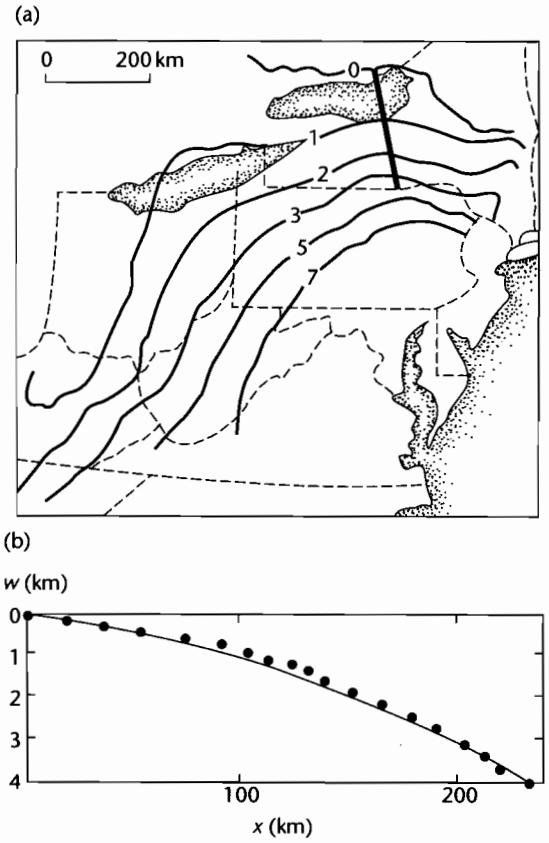

Fig. 4.9 Contours of basement (in km) in the Appalachian basin of the eastern United States, based on borehole records and seismic reflection studies (Turcotte and Schubert 1982, p. 131); (b) Depths of basement below sea level along the profile given in (a) as a function of distance from the point at which the basement rocks crop out at the surface. The heavy line is the theoretical deflection given by the universal flexure equation with $x_b - x_0$ equal to 122 km and w_b equal to 0.29 km.

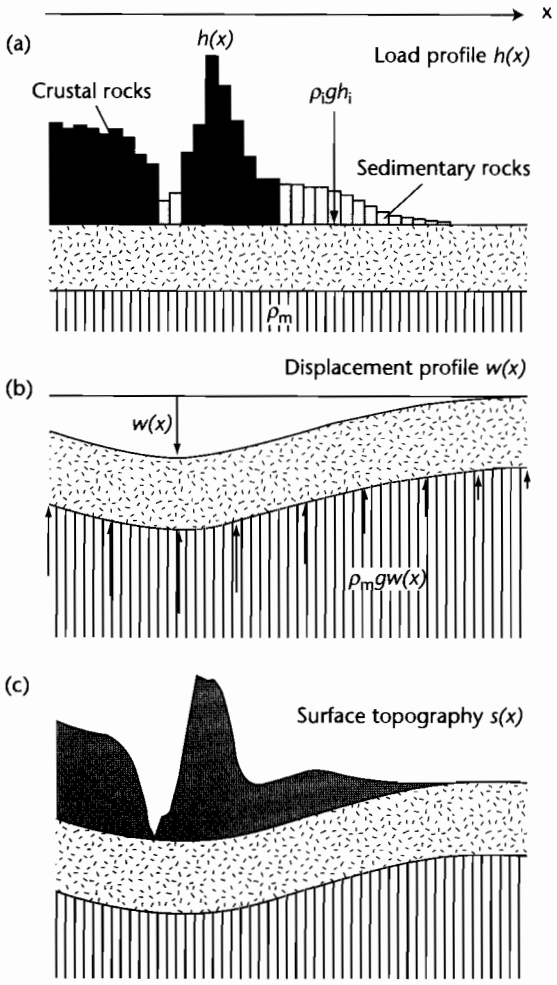

Fig. 4.10 Flexure under a distributed load. (a) The individual deflections caused by load blocks of given height h, density ρ, and width are solved analytically, and summed to give the displacement profile $w(x)$ in (b). The upward restoring force is shown by arrows. The distributed load then "sinks" into this displacement profile to give the resultant topographic profile $s(x)$ (c). Based on Jordan (1981) and Cardozo and Jordan (2001).

sider the solution of the general flexural equation for the case of an applied load $q_a(x)$.

Jordan (1981) made an early attempt to forward model the deflection of the continental lithosphere in the western interior of USA during the Late Jurassic–Cretaceous Sevier orogeny using a distributed load system on a linear elastic plate. The crustal loads were approximated by rectangular blocks of density ρ_c, with their centers s situated at a distance x km, half-width a, and height above sea level h (Fig. 4.10). These crustal blocks float on a fluid mantle with density ρ_m. The deflection of each load block w_i is calculated using a solution of the universal flexure equation. The sum of the deflections from all of the rectangular crustal blocks gives the total deflection. Jordan (1981) moved the crustal blocks to represent different stages in the evolution of the Sevier

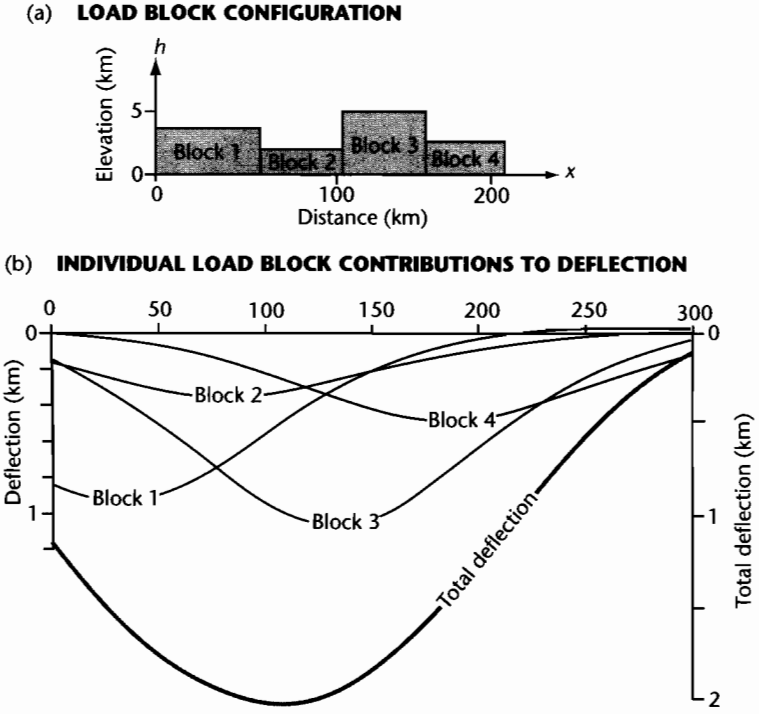

Fig. 4.11 Example of the individual deflections from a number of spatially distributed load blocks of crustal density (a), showing their mutual interference and total deflection (b). Flexural rigidity of $D = 10^{23}$ Nm.

orogen. For our purposes, we need only initially consider the static solution (Boxed text 4.1).

The deflections from a series of load blocks for a flexural rigidity of 10^{23} Nm is shown in Fig. 4.11. It is clear that the deflections of widely separated crustal blocks may destructively interfere.

The basins adjacent to eroding thrust belts are commonly filled with sediment. This sediment also acts as a vertically applied load on the continental lithosphere. The sedimentary infill of the basin can also be treated as a series of rectangular loads with height h_i and density ρ_i. The sum of the load profile $h(x)$ and the deflection profile $w(x)$ gives a topographic profile (Fig. 4.10). This type of 2-D modeling has been applied to the Tertiary Bermejo foreland basin of Argentina (Cardozo and Jordan 2001) and the Triassic Sichuan foreland basin of China (Yong et al. 2003).

A Matlab exercise to calculate the deflection caused by a distributed load can be found at www.erdw.ethz.ch/Allen.

4.3 FLEXURAL RIGIDITY OF OCEANIC AND CONTINENTAL LITHOSPHERE

4.3.1 Controls on the flexural rigidity of oceanic lithosphere

The lithosphere can be regarded as a thermal boundary layer losing heat to the atmosphere and oceans by conduction. The oceanic lithosphere thickens as a function of age, being ~6 km at ridge axes and thickening to about 100 km under the oldest (Jurassic) ocean floor (§2.2). Clearly, the ability of the oceanic lithosphere to support loads should also therefore be a function of its age. However, analysis of the flexure of the oceanic lithosphere at the Hawaiian–Emperor seamount chain (Watts 1978) suggested that equivalent elastic thicknesses were large at the old (75–80 Ma) end of the chain near the northernmost Emperor seamount, but low at the young (0–5 Ma) end near Hawaii, despite the fact that the age of the underlying oceanic crust (80–100 Ma) differs very

BOXED TEXT 4.1: Deflection under a Distributed Load

The deflection produced by each load i is given by the following set of equations (Heténi 1979; Jordan 1981).

If x is situated in the basin outboard from the load:

$$w_i = \frac{h}{2}\frac{\Delta\rho_1}{\Delta\rho_2}\left\{\begin{array}{l}\exp(-\lambda(x-s+a))\cos(\lambda(x-s+a)) \\ -\exp[-\lambda(x-s-a)]\cos[\lambda(x-s-a)]\end{array}\right\} \quad (4.13)$$

where

$\Delta\rho_1 = \rho_c - \rho_{air}$

$\Delta\rho_2 = \rho_m - \rho_{air}$

λ is an inverse flexural parameter ($1/\alpha$) (see equation 4.3), and $\Delta\rho$ is the density difference between mantle and air, and s is the position of the centre of the load, a is its half-width and h its height.

If x is under the load:

$$w_i = -\frac{h}{2}\frac{\Delta\rho_1}{\Delta\rho_2}\left\{\begin{array}{l}2-\exp[-\lambda(x-s+a)]\cos[\lambda(x-s+a)] \\ -\exp[-\lambda(-x+s+a)]\cos[\lambda(-x+s+a)]\end{array}\right\} \quad (4.14)$$

If x is situated behind (to the left of) the load block:

$$w_i = -\frac{h}{2}\frac{\Delta\rho_1}{\Delta\rho_2}\left\{\begin{array}{l}\exp[-\lambda(-x+s-a)]\cos[\lambda(-x+s-a)] \\ -\exp[-\lambda(-x+s+a)]\cos[\lambda(-x+s+a)]\end{array}\right\} \quad (4.15)$$

The total deflection resulting from the distributed load is found by summing the individual deflections w_i.

little along the length of the chain. In other words, volcanoes deflected oceanic lithosphere of different ages *at the time of loading*. A plot of 139 estimates of the elastic thickness of the oceanic lithosphere against age of the lithosphere at the time of loading (Fig. 4.12) (Watts 2001, p. 242) shows that oceanic flexural rigidity expressed as an equivalent elastic thickness (T_e) is approximated by the depth to the 300–600 °C isotherm. The lithosphere becomes stronger with the age of the lithosphere at the time of loading. This relationship is exponential with time, similar to that of the oceanic bathymetry using a cooling plate model such as that shown in Fig. 2.20 (Parsons and Sclater 1977). The evidence therefore suggests that the oceanic lithosphere can be treated as being elastic rather than viscoelastic (Watts et al. 1982) (§2.4.4) with a flexural rigidity dependent on its age at the time of loading. However, it is apparent from Fig. 4.13 that there is considerable scatter. Such variation may be due to viscoelastic effects in a multilayered oceanic lithosphere.

Although investigation of the oceanic lithosphere allows us to lay down some fundamental concepts in flexure, it is of little importance in basin analysis, since most sedimentary basins of interest to us are formed on continental lithosphere. It is therefore important to understand what controls the flexural rigidity of continental lithosphere.

4.3.2 Flexure of the continental lithosphere

4.3.2.1 Introduction

The continental elastic lithosphere responds differently to the oceanic elastic lithosphere on all scales of deformation. The continents appear to accumulate strains over long periods of geological time whereas the oceanic lithosphere remains relatively intact over its short lifetime of up to about 180 Myr. This is illustrated by the presence of narrow and well-defined plate boundaries in the oceans as opposed to the wide and diffuse zones in the continents such as the Himalayas and Tibet (reviewed in Molnar 1988). The continents are therefore exceedingly complex, particularly in their inherited fabric. In addition, strength profiles of the continental lithosphere show two high strength zones and two brittle–ductile transitions (§2.4.6). A four-layer lithosphere is unlikely to behave in a simple fashion when subjected to an applied load system. The flexure of continental lithosphere is therefore controversial. Some workers have proposed that there is a correlation in Eurasia between the equivalent elastic thickness of the continental lithosphere (derived from gravity anomalies and topography) and the thickness of the seismogenic crust (Maggi et al. 2000). However, this correlation is not substantiated elsewhere (e.g., Cardozo and Jordan

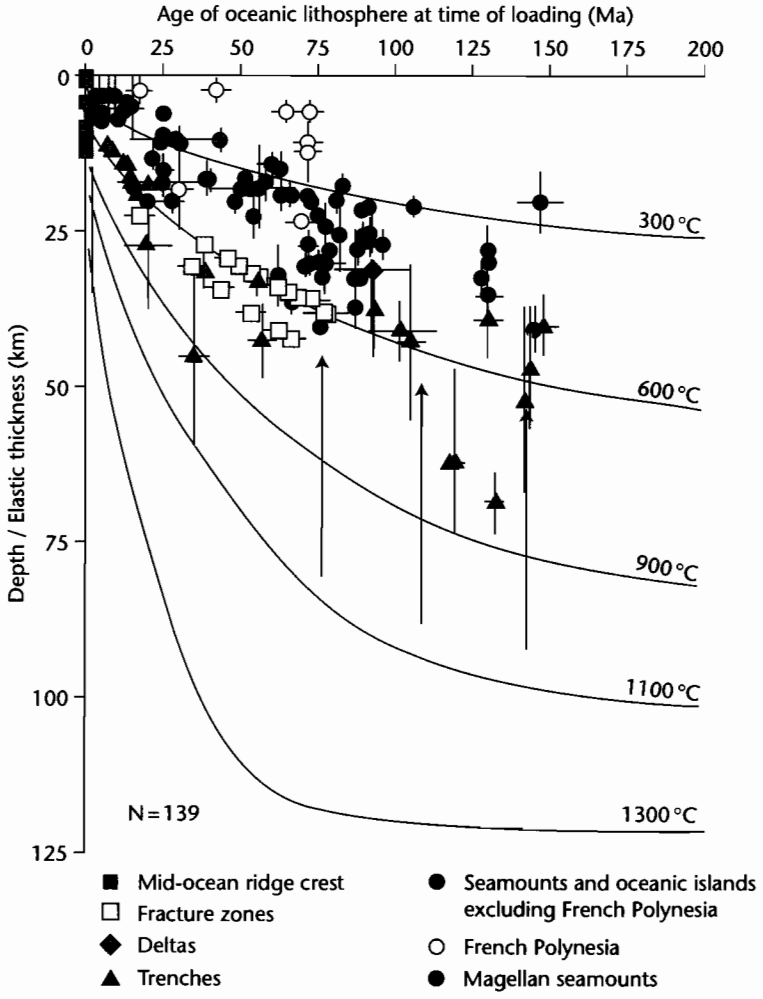

Fig. 4.12 Plot of the flexural rigidity of the oceanic lithosphere (expressed as equivalent elastic thickness *Te*), as a function of its age at the time of loading (after Watts et al. 1982, updated in Watts 2001). The equivalent elastic thickness estimates are shown for mid-ocean ridges and fracture zones, seamounts and oceanic islands, trenches and deltas. Isotherms are for a cooling plate model (Parsons and Sclater 1977), showing that most data fall within the 300 °C to 600 °C isotherms. The general relationship is that equivalent elastic thickness increases with the age of the oceanic lithosphere at the time of loading. Reproduced courtesy of Cambridge University Press.

2001) and there are no simple measurable parameters that can be confidently correlated with the observed flexural rigidity of the continental lithosphere (McNutt et al. 1988) (discussed below). The change through time ("secular evolution") of the flexural rigidity of continental lithosphere has in particular been widely discussed.

4.3.2.2 Controls on the flexural rigidity of the continental lithosphere

The elastic plate thicknesses (or flexural rigidities) for continental lithosphere have been calculated in a wide variety of tectonic settings. Flexural rigidities have been

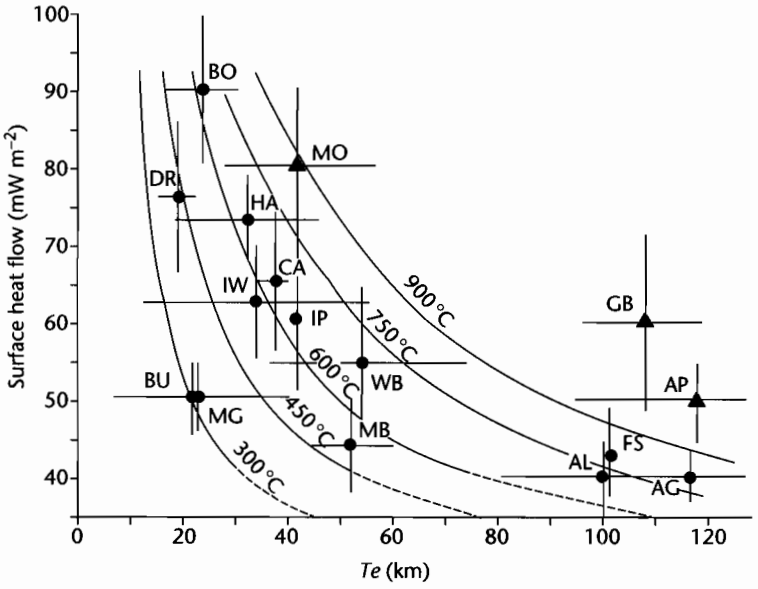

Fig. 4.13 Plot of the equivalent elastic thickness *Te* versus surface heat flow for a number of sites of flexure. The solid curves indicate depths to isotherms at a given surface heat flow for a steady state thermal model. The plot demonstrates the very wide range in temperature (300 °C to >900 °C) for the base of the elastic lithosphere. Flexure sites are as follows: AG, Lake Agassiz; AL, Lake Algonquin; FS, Fennoscandia; CA, Caribou Mountains; IP, Interior Plains; GB, Ganges Basin; IW, Idaho–Wyoming thrust belt; MB, Michigan Basin; BU, Boothnia Uplift; MG, Midcontinent gravity high: HA, Lake Hamilton; BO, Lake Bonneville; DR, North Great Dividing Range; AP, Appalachian Foreland Basin; MO, Molasse Basin; WB, Williston Basin (full details in Willett et al. 1985).

estimated from late glacial rebound, such as in Pleistocene Lake Bonneville (Crittenden 1963; Nakiboglu and Lambeck 1983), Lake Agassiz (Walcott 1970), and Fennoscandia (McConnell 1968). Estimates have also been obtained from regions of lithospheric extension such as the rifts of the East African Rift System (Banks and Swain 1978; Bechtel et al. 1987; Ebinger et al. 1991; Upcott et al. 1996), the North Sea (Kusznir et al. 1991) and Rhine Graben (Weissel and Karner 1989), and at passive continental margins, particularly that of the eastern seaboard of the USA–Canada (Watts 1988; Keen and Dehler 1997). By far the greatest data set, however, comes from the flexure of the continental lithosphere at foreland basins (Table 4.1).

Whereas, to a first approximation, the loading of oceanic and continental lithosphere can be modeled as a flexed elastic plate overlying a fluid substratum, laboratory-derived rock deformation data (Goetze 1978; Goetze and Evans 1979; Kirby 1983) show that the true rheology of the lithosphere is far more complex. Karner et al. (1983) applied a thermo-elastic rheologic model to the flexure of continental lithosphere and concluded that in terms of flexural rigidity, the results from oceanic and continental lithosphere were compatible. They believed that the long-term thermal behavior of the continental lithosphere is governed by a simple cooling plate model (plate thickness of 200–250 km), and that the effective elastic thickness for continental lithosphere corresponds with the depth to the 450 °C isotherm, and does not change following loading.

Others claim that there is no clear relation between thermal state and age of continental lithosphere, and that the effective elastic thickness does not correspond to the 450 °C isotherm, but rather spans a wide temperature range of 300 °C to >900 °C (Fig. 4.13). Willett et al. (1985) instead suggested a Maxwell viscoelastic heterogeneous lithosphere, i.e., a nonlinear thermally activated rheology (see §2.3.4), with viscous strain rates in the lithosphere determined by a power law ($n = 3$). In such a model, the deviatoric stress resulting from a supralithospheric load initially increases toward the base of the mechanical lithosphere, but immediately after loading,

Table 4.1 Equivalent elastic thickness (T_e) compiled by Watts (2001) for the continental lithosphere at sites of foreland basins. Particular foreland basins may appear more than once if estimates have been made by different authors. Sources given in Watts (2001, Table 6.2, pp.251–3).

Site	Age of plate (Ma)	Plate age error (Myr)	Age of load (ka)	Load age error (kyr)	*Te* (km)	*Te* error (km)
Idaho–Wyoming	2650	50	125	25	22.0	0.0
Alps East	350	50	110	0	50.0	10.0
Alps West	275	25	110	0	25.0	10.0
Appalachians	1050	50	375	75	105.0	25.0
Himalaya East	1200	500	52	2	90.0	10.0
Ganges	1500	500	52	2	86.5	25.0
Kunlun–Tarim	800	200	52	2	40.0	5.0
Apennines	300	50	5	0	11.5	6.5
Carpathians Southeast	1600	200	110	0	30.0	10.0
Bolivian Andes	950	350	60	0	45.0	20.0
Transverse Ranges S	100	0	50	0	10.0	10.0
Transverse Ranges N	100	0	50	0	50.0	0.0
Zagros	700	200	35	10	50.0	25.0
Ebro	275	25	40	5	18.6	6.9
Aquitaine	275	25	40	5	25.5	5.0
Colville	1900	100	140	20	65.0	5.0
Carpathians	1600	200	110	0	22.0	0.0
Calabria	300	50	2	2	18.7	4.7
Urals	1500	100	325	50	75.0	25.0
Apennines	300	50	5	0	20.0	5.0
Oman	700	200	85	10	13.0	3.0
Urals	1500	100	325	50	75.0	25.0
Verkhoyansk	1950	150	230	40	50.0	10.0
Pamir	300	100	52	2	15.0	5.0
Tien Shan Tarim	800	200	52	2	40.0	20.0
Sicily	275	25	25	0	6.0	4.0
Himalaya West	1200	500	52	2	34.0	6.0
Greater Caucasus	1600	200	100	0	45.0	5.0
Kilohigok	2575	75	1965	45	12.0	4.0
Thelon front	2575	75	2000	0	58.0	0.0
Grenville front	2700	100	1050	50	126.0	0.0
Labrador Trough	2575	75	1585	50	120.0	0.0
Cape Smith	2575	75	1800	50	74.0	0.0
New Guinea East	700	100	25	0	10.0	0.0
New Guinea West	700	100	25	0	75.0	25.0
Tarim	1800	50	900	50	55.0	5.0
Ebro	275	25	40	0	20.0	0.0
Dzhungarian	1800	50	900	50	12.5	12.5
Alps West	275	25	17	0	10.0	5.0
Po Basin	275	25	30	0	5.0	0.0
Apennines	300	50	5	0	6.3	2.2
Guadalquivir Betics	275	25	25	0	10.0	5.0
Apennines	300	50	5	0	20.0	0.0
Carpathians	1600	200	110	0	40.0	0.0
Hellenides	300	50	2	2	70.0	0.0
Himalayas	1200	500	52	2	80.0	0.0
East Alps	350	50	110	0	40.0	0.0
South Alps	300	50	110	0	20.0	0.0

Table 4.1 *Continued*

Site	Age of plate (Ma)	Plate age error (Myr)	Age of load (ka)	Load age error (kyr)	*Te* (km)	*Te* error (km)
West Alps	275	25	110	0	50.0	0.0
South Alps	300	50	110	0	15.0	0.0
Apennines	300	50	5	0	15.0	0.0
Oman	700	200	85	10	35.0	13.0
Apennines–Dinarides Plio–Quaternary	300	50	2	2	12.5	2.5
Apennines–Dinarides Eocene–Oligocene	300	50	40	5	7.5	2.5
Kopet Dag	1600	200	52	2	25.0	5.0
Karakorum India	1200	500	52	2	90.0	10.0
Karakorum Asia	1200	500	52	2	110.0	10.0
Andes Peru	950	350	60	0	39.0	16.0
Himalaya East	1200	500	52	2	90.0	0.0
Tarim	1800	50	900	50	40.0	0.0
Atlas East	300	50	25	0	20.0	1.0
Atlas West	300	50	25	0	9.0	1.0
Appalachians	1050	50	375	75	70.0	20.0
Alps East	350	50	110	0	25.0	10.0
Alps West	275	25	110	0	10.0	5.0
Carpathians Southeast	1600	200	110	0	12.0	8.0
Andes Colombia	950	350	80	0	45.0	40.0
Andes Equador	950	350	80	0	25.0	20.0
Andes North Peru	950	350	60	0	35.0	35.0
Andes Peru	950	350	60	0	25.0	20.0
Andes Peru–N. Chile	950	350	60	0	45.0	40.0
Andes Argentina	950	350	60	0	30.0	20.0
Ouachita	1050	50	375	75	50.0	10.0
E. Papua New Guinea	97	32	30	5	20.0	10.0
W. Papua New Guinea	387	132	30	5	75.0	5.0

viscous relaxation causes stresses to be progressively concentrated in the colder upper lithosphere. Any surface deflection should deepen and narrow with time since loading, but at long times after loading, the stress field and surface displacements do not change significantly, suggesting that there is a long-term asymptotic elastic thickness (see also Kusznir and Karner 1985). The orogenward migration of the flexural forebulge of the Appalachian foreland basin system has been interpreted as evidence for viscoelastic relaxation (Quinlan and Beaumont 1984; Tankard 1986).

A plot of flexural rigidity/elastic thickness of the continental lithosphere versus thermal age, or versus the age at the time of loading, using the most complete data set currently available (Watts 2001), shows no global relationship (Fig. 4.14). Values appear to range between <5 km and 110 km with no clear modes at particular depth ranges, although rift provinces tend to have values of *Te* of <30 km. There clearly must be other factors contributing strongly to the value of the flexural strength of the lithosphere. One factor is the present day geothermal gradient, which is strongly influenced by the concentration of radiogenic heat-producing elements in the crust (Pinet et al. 1991). If continental *Te* is determined by the depth to the 450 °C isotherm, variations in the continental geotherm would explain variations in the value of continental *Te*. Estimates of *Te* based on geothermal data in North America (Pinet et al. 1991) are supported by estimates of *Te* from admittance and coherence studies (Bechtel et al. 1990).

Other mechanisms affecting the flexure of the continental lithosphere are the possible *decoupling* of a strong

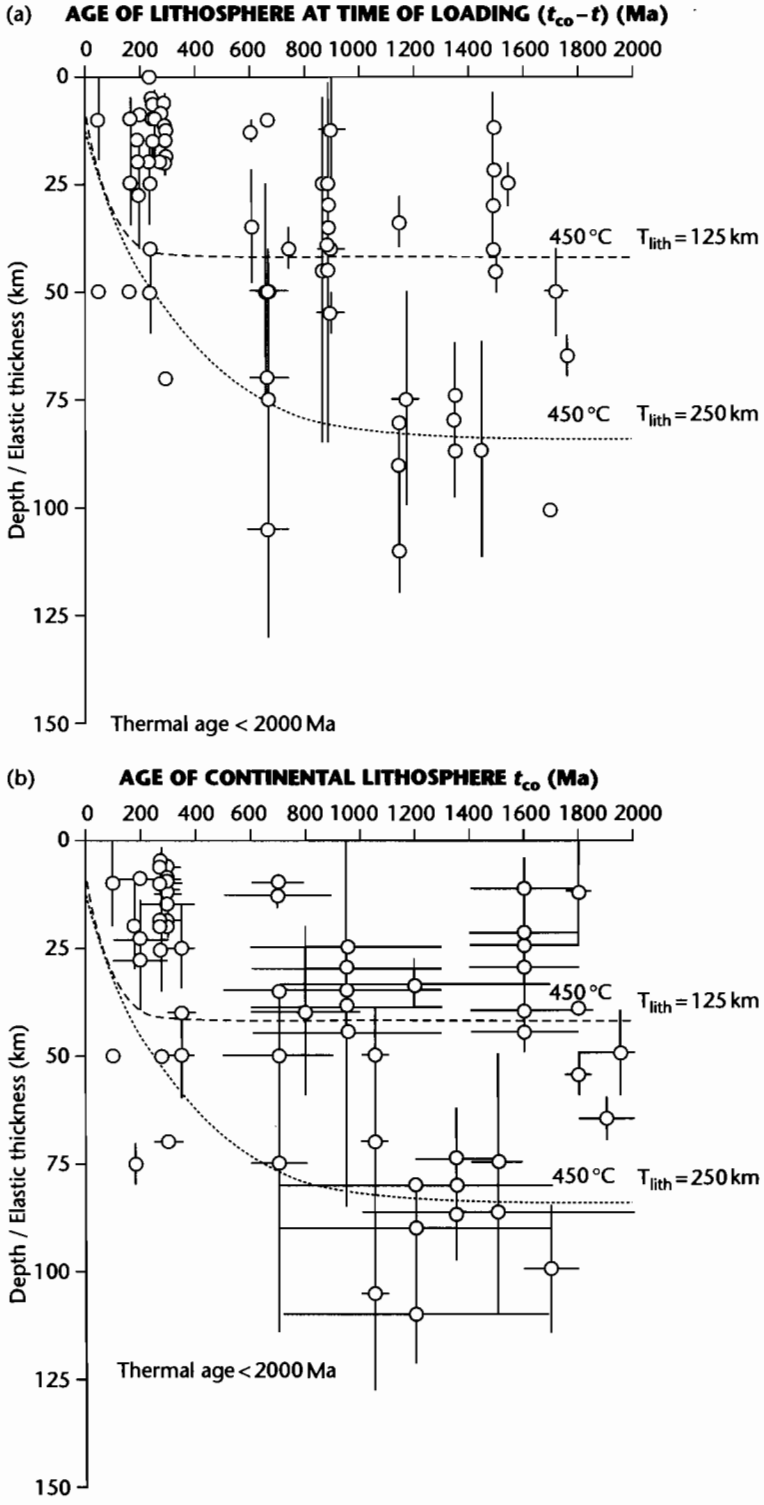

Fig. 4.14 Plots of flexural rigidity expressed as equivalent elastic thickness versus (a) age of the lithosphere at the time of loading and (b) age of the continental lithosphere, for 66 foreland basins and 6 late glacial rebound sites (after Watts 2001). Note that there is no correlation for this continental dataset. Reproduced courtesy of Cambridge University Press.

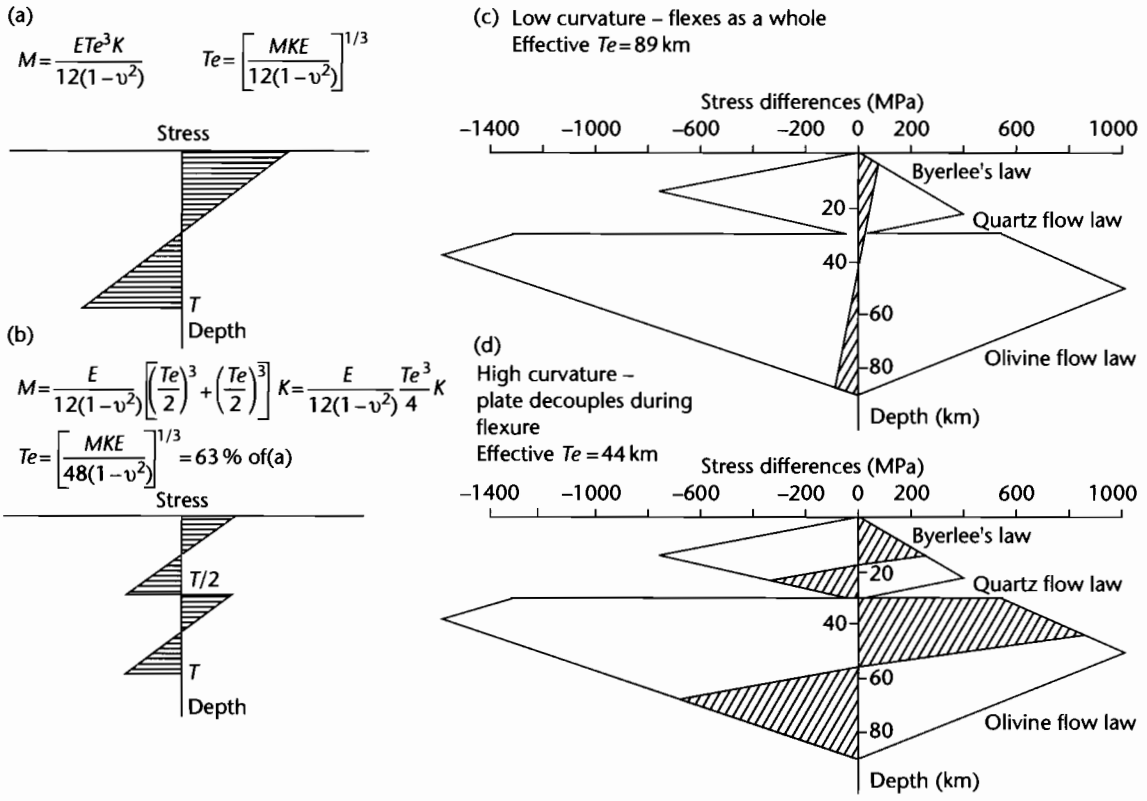

Fig. 4.15 The effects of decoupling at high curvatures illustrated by cross-sections of stress in the flexed lithosphere (after McNutt et al. 1988). (a) Distribution of fiber stresses in an elastic plate of thickness T showing extension in the upper half of the plate and compression in the lower half; (b) A purely elastic plate that is decoupled at $T/2$ so that the upper and lower portions flex independently with the same radius of curvature as in (a). The equivalent elastic thickness is 63% of that in (a). M is the bending moment, K the radius of curvature, E Young's modulus, υ Poisson's ratio; (c) and (d) Rheologically layered continental lithosphere showing the failure envelope under extension (positive stress) and compression (negative stress). The strength is limited by frictional sliding (Byerlee's law) in the upper crust and uppermost mantle and by ductile flow in the lower crust and lower lithosphere. The hatched areas represent the stress resulting from flexure superimposed on the failure envelope. In (c) the plate is flexed at a very low curvature. The fiber stresses rarely exceed the failure criterion of the plate (there is a small amount of yielding at the top and bottom) and the equivalent elastic thickness (89 km) is almost exactly the same as the thickness of the elastic plate. In (d) the plate is flexed to a high curvature. This leads to the failure criterion being exceeded and a decoupling zone forms in the lower crust. The equivalent elastic thickness calculated for the total bending moment sustained in both the crust and the mantle is just 44 km. Decoupling therefore has strong potential mechanical implications for flexure.

upper crust from a strong underlying mantle during plate bending (Fig. 4.15) (Burov and Diament 1995; Lavier and Steckler 1997). Where the lithosphere is young and hot, it is prone to decoupling, thereby explaining the low Te in regions such as the Apennines and Alps. Where the lithosphere is old and cold, the lithosphere does not decouple, which explains the high Te in regions such as the Himalayas. Lavier and Steckler (1997) stress the role of sediment blanketing in raising temperatures high enough to cause weakening, yielding, and therefore decoupling.

The concept of a yield strength envelope (§2.4.6) suggests that if stresses caused by loading exceed the strength of the lithosphere, it will *yield* rather than flex elastically

(Fig 4.15). The yielding of a flexed plate should be related to its curvature (Goetze and Evans 1979). Initially as curvature increases (beyond *c.* $10^{-7}\,m^{-1}$), the upper and lower parts of the plate should yield, thereby reducing its elastic thickness. Measurements at ocean trenches indicate curvatures from 1×10^{-6} to $8 \times 10^{-7}\,m^{-1}$, suggesting that some yielding should be taking place (McNutt 1984).

McNutt and Kogan (1987) believed there was a good correlation between the elastic plate thickness and the surface curvature in map view of the thrust belts of mountain ranges. Highly arcuate mountain belts are associated with low elastic thicknesses (Alps, Carpathians) whereas long linear belts tend to be supported by a strong plate (Urals, Appalachians). The highly arcuate belts are commonly associated with back arc extension (e.g., Pannonian Basin), itself related to the dip of the subducting slab (Uyeda and Kanamori 1979). McNutt and Kogan (1987) suggested that the plan view shape is related to the cross-sectional curvature of the flexed plate, steeply dipping highly curved plates appearing weaker, and shallowly dipping plates appearing stronger. This would imply that the equivalent elastic thickness is not so much related to a characteristic isotherm, but is more due to the extent to which the elastic lithosphere has flexed under high bending stresses.

McNutt et al. (1988) analyzed 15 mountain belts and concluded that there was no indication that older mountain belts had experienced viscoelastic relaxation causing their present flexural rigidities to be low. The age of the continental lithosphere at the time of loading appears to set an upper bound to the maximum possible equivalent elastic thickness that can be observed. However, many *Te* values fall well below this level, suggesting that some weakening has taken place, but regardless of plate age. As introduced above, this mechanism of weakening may be related to *decoupling* or to *yielding*, reducing the effective elastic thickness from the purely elastic case by a factor of up to 2.

It could be argued that the curvature of thrust belts is more strongly influenced by variations in the mechanical properties of the stratigraphy and shallow basement being deformed, rather than scaling on the rigidity of the underlying plate. Sinclair (1996) therefore plotted equivalent elastic thickness estimates versus the curvature of the foreland basin's outer margin using carefully screened examples (see discussion in Zweigel and Zweigel 1998). He found a linear relationship, supporting the idea that weak plates correlate with arcuate mountain belts and foreland basins (McNutt et al. 1988).

4.3.2.3 Spatial and secular variations in flexural rigidity

It was noted in §4.1 and §4.2 how gravity data can be used to constrain flexural models of the oceanic lithosphere at mid-plate seamount chains and deep-sea trenches. Gravity (Bouguer) anomalies have also been widely used to study the flexure resulting from continental collision (Karner and Watts 1983; Lyon-Caen and Molnar 1989; Stewart and Watts 1997). Commonly used techniques include the matching of observed Bouguer gravity measurements with predictions forward modeled for different values of flexural rigidity, and spectral methods using the coherence and admittance of the Bouguer gravity field with topography (see §2.3.3). Watts (2001) gives a detailed account.

Bouguer gravity data allow a comparison between the observed deflection and the topographic loads of mountain belts. For example, Bouguer gravity anomalies along profiles in the western Himalaya and Ganga Basin indicate a mass deficit over the basin and a mass excess in the Lesser Himalaya (Lyon-Caen and Molnar 1985) (Fig. 4.4). The Bouguer anomaly over the Ganga Basin is, however, smaller than expected from the topographic load of the Himalaya, suggesting that some additional force, acting upward on the deflected lithosphere, is necessary. In contrast, the topographic load of the Zagros Mountains is insufficient to cause the observed flexure of the Arabian Plate with the formation of the Mesopotamian Foredeep and Persian Gulf as the foreland basin (Snyder and Barazangi 1986). This leads to the requirement for an additional force flexing the Arabian Plate downwards. Snyder and Barazangi (1986) believe that this additional force may be horizontal compression. It is less likely to be subsurface density variations caused by overriding an initially thinned Arabian continental margin, since there is no associated positive Bouguer anomaly, unlike in the Alps and the Appalachians (Karner and Watts 1983; Stewart and Watts 1997).

Profiles transverse to the axis of mountain belts commonly reveal significant variations in the flexural rigidity of the lower plate. Based on Bouguer gravity profiles, the flexural rigidity of the Indian Plate being overridden by the western Himalayas varies considerably over even relatively small horizontal distances (Lyon-Caen and Molnar 1985). Between profiles 200 km apart, estimated flexural rigidities changed by a factor of 5–10 (between *c.* 10^{24} and 7×10^{24} Nm), corresponding to a variation of equivalent elastic thickness by a factor of 2 (from

c. 54km to 104km). The rapidity of the horizontal changes suggests that flexural rigidity variations are not a result purely of differences in convective heat supply or loss in the mantle, but may instead be a result of small temperature variations causing large changes in strength in a highly temperature-dependent lithosphere, or of compositional or thickness changes of the deflected lithosphere. It is necessary to infer a segment of the Indian Plate, now deeply buried beneath the lesser Himalaya, which is steeply dipping and considerably weaker than the segment under the Ganga Basin (*c.* $2–5 \times 10^{22}$ Nm). This turns out to be a common feature of collision zones, since a similar abrupt steepening of the Moho is found in the Carpathian, Apennine, Alpine, Andean, and Zagros mountain belts.

The Alpine chain of Europe also shows strong variations in the estimated flexural rigidity derived from Bouguer gravity modeling (Stewart and Watts 1997). In particular, flexural rigidities appear to be low in western Switzerland, in close proximity to the Rhine Graben. Stewart and Watts (1997) therefore invoked a reduction of lithospheric strength by the thermal weakening of the plate in the region of the Rhine Rift.

Spatial variations in the flexural rigidity of the foreland plate may affect its response to moving applied loads during their migration history. The most likely scenario involves the closure of an ocean basin, causing initially the loading of the attenuated continental margin prior to full collision, when normal thickness continental lithosphere is flexed (Stockmal et al. 1986). Stewart and Watts (1997) identified such a strike normal increase in flexural rigidity with distance from the Andean orogenic belt in Ecuador using the Bouguer gravity field. In such a situation, with continued convergence the upper plate should initially deflect a weak lower plate, and then a progressively stronger lower plate. Although this is conceptually reasonable, there is no evidence of an increase in flexural rigidity of the European foreland plate during Alpine orogenesis from the marine (Late Eocene–Early Oligocene "flysch" stage to the predominantly nonmarine (Late Oligocene–Miocene) "molasse" phase (Allen et al. 2001) (see also §8.3.1).

4.3.3 Effects of plate segmentation during subduction

We have so far considered the deflection of the lithosphere at collision zones to be perfectly cylindrical. That is, any 2-D transect would be representative of the flexure as a whole. However, in some instances, there are offsets in the positions of the depocenters marking distinct foredeep segments. The Apennines of Italy are a well-documented example (Royden et al. 1987). Four forebulge segments, each characterized by Bouguer gravity highs can be distinguished (Fig. 4.16). They are thought to be linked to four slab segments delimited by tears or lines of weakness in the subducted slab. Along transects within individual segments, the gravity data can be used to calculate the equivalent elastic thickness of the plate. (The topographic loads on the plate are thought to be insufficient to explain the deflection (Royden and Karner 1984) and substantial subsurface loads are invoked that are several times the magnitude of the surface load.) In all four segments, the equivalent elastic thickness is in the range 15–20km (Royden et al. 1987), suggesting a uniform but stepped response of the deflected lithosphere. The stepped deflection is thought to be due to segmentation of the lithosphere within the subduction zone. The model deflection using a semi-infinite elastic sheet is illustrated in Figure 4.17. Applied loads and bending moments applied to the segments of the subducted lithosphere produced a series of offset forebulges and foredeep basin compartments that match well with the Apenninic geology. The segmentation of the plate at depth is masked by a continuous zone underlying the foreland basin, the only evidence for the segmentation lying in the distribution of the swells and basins on the deflected plate.

Furthermore, the thrust belt appears to mimic the deeper segmentation. In the segment with a forebulge far to the northeast, the thrust belt has also advanced relatively far to the northeast. In contrast, the lesser-traveled thrust units are correlated with forebulges relatively to the southwest. Since subsurface loads (i.e., forces within a subduction zone) are thought to be much more important than surface loads in the Apennines, this implies that near-surface tectonics are also intimately related to lithospheric heterogeneity at depth.

4.4 LITHOSPHERIC BUCKLING

Long wavelength folding or *buckling* of the lithosphere has been suggested for the Indian Ocean and central Australia (Fleitout and Froideveaux 1982; Lambeck 1983), but the wide applicability to the continents has been in some doubt. Long wavelength folding of the continental lithosphere has now been suggested from several continents (central Australia, central Asia, Canada,

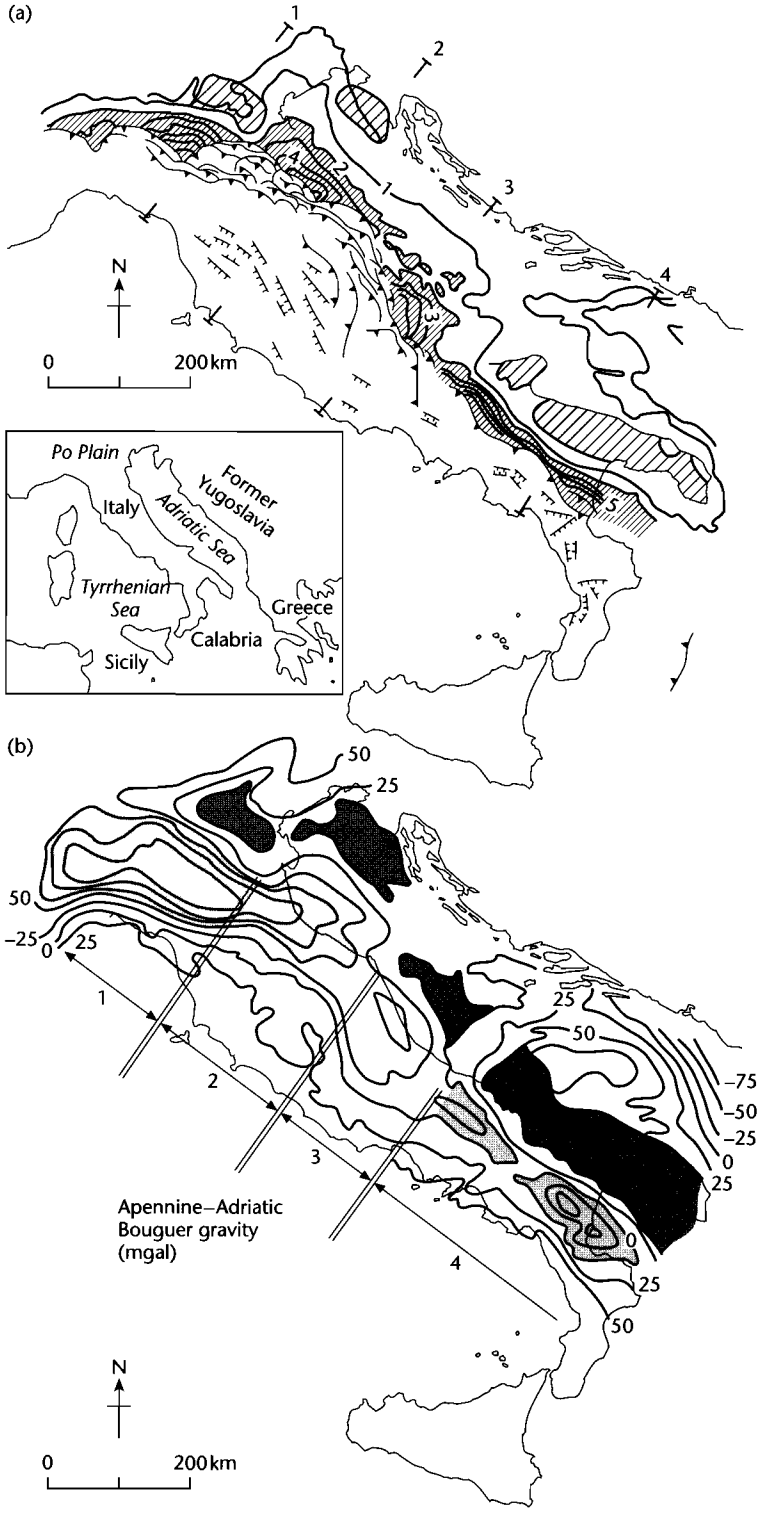
(a)
1
2
3
4
5
N
0
200 km
Po Plain
Italy
Former Yugoslavia
Adriatic Sea
Tyrrhenian Sea
Greece
Calabria
Sicily
(b)
50
25
0
–25
–50
–75
1
2
3
4
Apennine–Adriatic
Bouguer gravity
(mgal)
N
0
200 km

western Europe) (references and details in Cloetingh et al. 1999). The typical wavelengths observed are 50–600 km. If lithospheric buckling of significant amplitude takes place, it is important to recognize it and to discriminate it from the effects of lithospheric flexure due to the predominantly vertically applied loads in mountain belts. In this section, linear elastic theory is developed for the case of buckling of an elastic sheet embedded between an overlying ocean and an underlying fluid-like mantle (Boxed text 4.2). We then explore the inadequacies of this approach when applied to the case of the real continental lithosphere subjected to in-plane compressive stresses.

4.4.1 Theory: linear elasticity

We have previously seen that the lithosphere flexes under an applied system that may include vertically applied distributed loads, torques and horizontal loads (§2.1.4, §4.2). The question has not yet been addressed of whether the lithosphere is able to buckle under large horizontal, in-plane forces. We first approach this problem using an elastic beam under horizontal compression, and then extend the analysis to a lithosphere with an upward restoring force (see Boxed text 4.2).

We are now in a position to find out if the lithosphere should buckle under an in-plane stress. We take the following parameter values: Young's modulus $E = 70\,\text{GPa}$, Poisson's ratio $\nu = 0.25$, mantle density $\rho_m = 3300\,\text{kg m}^{-3}$, and ocean water density $\rho_w = 1000\,\text{kg m}^{-3}$, elastic plate thickness $h = 50\,\text{km}$. This gives a critical stress for buckling of 5.3 GPa, which is far too high for the brittle part of the lithosphere to withstand without faulting. If we reduce the elastic thickness and cover the elastic lithosphere by a sedimentary layer, thereby reducing the density difference $\Delta\rho$, the critical stress for buckling

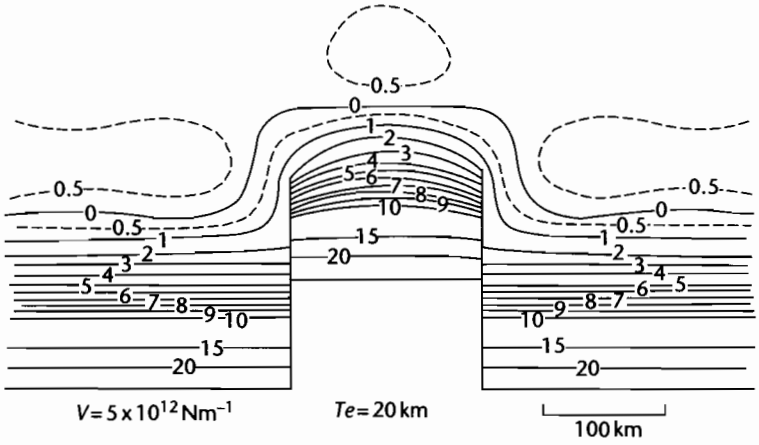

Fig. 4.17 Three-D model used by Royden et al. (1987) to simulate the flexure of segmented lithosphere. The lithosphere is assumed to be continuous in the foreland region but to be segmented by free boundaries or faults in the subduction zone. Vertical loads and/or bending moments are applied to the ends of the broken segments of the plate. The contours of the deflected surface, assuming the three slab segments to be initially at 1 km depth, are shown in km. A uniform equivalent elastic thickness of 20 km is assumed throughout and the vertical end load is $5 \times 10^{12}\,\text{Nm}^{-1}$. Note the offset of the outer rise segments and the 3-D pattern of the foreland basin depocenters.

Fig. 4.16 (a) General map of the Apennine system showing depth to the base of the Pliocene in the Adriatic and Po basins at a 1 km contour interval. There are four distinct outer rise/forebulge segments recognized in the basal Pliocene surface (shown in wide diagonal hatch). The narrow diagonal hatch shows the Apennine foreland basin and parts of the basal Pliocene surface that is below 2 km in depth; (b) Simplified map of the Bouguer anomaly gravity field (milligals). Contour interval is 25 mgal. The four morphological outer rises correspond to Bouguer gravity highs, suggesting that they are maintained by regional flexure. The shaded areas represent anomalies of greater than 0 mgal in sectors 1 to 3 and 50 mgal in sector 4: stipple shows gravity anomalies less than −50 mgal in sectors 1 to 3 and 0 mgal in sector 4. These sectors are believed to be bounded by major tears in the subducted plate, segmenting it at depth (after Royden et al. 1987, compiled from Ogniben et al. 1975, and Morelli et al. 1975).

BOXED TEXT 4.2: Buckling of an Elastic Beam

Initially, consider a beam fixed at its ends so that there are no applied torques (Fig. 4.18). The solution to the deflection of the beam under a horizontal load P is given by the general flexure equation (eqn 2.27). Integrating this equation twice with the boundary conditions that $w = 0$ at $x = 0$, $x = L$ and $d^2w/dx^2 = 0$ at $x = 0$ and $x = L$, gives

$$\lambda_c = 2\pi\left\{\frac{Eh^3}{12(1-\nu^2)(\rho_m-\rho_w)g}\right\}D\frac{d^2w}{dx^2}+Pw=0 \qquad (4.16)$$

This equation has the general solution

$$w = c_1\sin\left(\frac{P}{D}\right)^{1/2}x + c_2\cos\left(\frac{P}{D}\right)^{1/2}x \qquad (4.17)$$

where c_1 and c_2 are constants of integration. Equation 4.17 can be solved for the above boundary conditions to give

$$P = \frac{n^2\pi^2}{L^2}D \qquad (4.18)$$

where n is an integer multiple of π. The minimum horizontal load required to buckle the beam is when $n = 1$, in which case

$$P = P_c = \frac{\pi^2}{L^2}D \qquad (4.19)$$

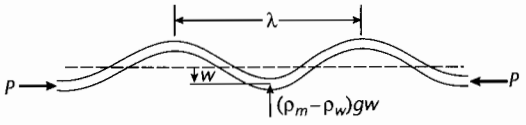

Fig. 4.18 Buckling of an infinitely long plate under an applied horizontal load with an upward restoring force (see Turcotte and Schubert 2002).

If P is smaller than the critical value P_c, the plate will not deflect under a horizontal load. If P is larger than P_c, the plate buckles, and its shape is half a sine curve of the form

$$w = c_1\sin\left(\frac{P}{D}\right)^{1/2}x = c_1\sin\frac{\pi x}{L} \qquad (4.20)$$

where c_1 is a constant relating the deflection to the horizontal force P.

This is not a realistic model of the lithosphere, since no restoring forces are exerted by underlying or overlying layers. The general flexure equation needs to be modified to incorporate the effects of an upward restoring force (eqn 2.28). The sinusoidal form of the deflection is of the form

$$D\left(\frac{2\pi}{\lambda}\right)^4 - P\left(\frac{2\pi}{\lambda}\right)^2 + (\rho_m-\rho_w)g = 0 \qquad (4.21)$$

where λ is the wavelength of the deflection and ρ_m and ρ_w are the mantle and water densities respectively. The solution (Turcotte and Schubert 2002, p. 124) is expressed in the form of the critical horizontal force to cause buckling as

$$P_c = \{4Dg(\rho_m-\rho_w)\}^{1/2} \qquad (4.22)$$

It is more convenient to express this critical horizontal force in terms of the critical horizontal stress and elastic plate thickness h, giving

$$\sigma_c = \left(\frac{Eh(\rho_m-\rho_w)g}{3(1-\nu^2)}\right)^{1/2}. \qquad (4.23)$$

The wavelength at the onset of buckling is

$$\lambda_c = 2\pi\left\{\frac{Eh^3}{12(1-\nu^2)(\rho_m-\rho_w)g}\right\} \qquad (4.24)$$

reduces (by about 75%) to slightly more realistic values. However, the wavelength at such reduced critical stresses is ≪50 km. This analysis suggests that although thin elastic layers embedded in surrounding rocks may deform by buckling, large scale, whole lithosphere folding should not occur in nature.

4.4.2 Lithospheric buckling in nature and in numerical experiments

The foregoing analysis highlights a problem. Unrealistically high stresses are required to initiate lithospheric buckling when it is treated using linear elasticity. Yet observations suggest that long wavelength buckles are common in the continental lithosphere, and develop early during phases of shortening in distant mountain belts. Sedimentary basins of central Australia, central Asia, the Himalayan perimeter, and Iberia have all been interpreted in terms of long wavelength lithospheric buckling. Basins with a previous extensional history are also believed to have been modified by in-plane stresses causing buckling (Ziegler et al. 1995).

Lithospheric folding is largely controlled by rheologic and thermal structure. The initial crustal thickness and thermal state of the lithosphere are therefore very important in determining the effectiveness of far-field compressive stresses (Cloetingh and Burov 1996). Consequently, different responses to compressive forces are expected in the relatively warm Alpine foreland of Europe compared to the relatively cold lithosphere of the Russian Platform because of their different strength profiles. In addition, buckling can be initiated at much lower compressive in-plane stresses with an elastic–ductile rheology than with a linear elastic rheology.

Cloetingh et al. (1999) recognized different types of long wavelength folding:

1 *Regular or periodic folding* is inferred from undulations of the "basement" imaged by seismic reflection and refraction, variations of Bouguer gravity anomalies and periodic vertical tectonic movements. Most cases of regular folding occur in young, weak lithosphere, which is strongly affected by horizontal loads. Long wavelength warping is occasionally detected by geomorphic observations such as the tilting of river terraces. Numerical experiments suggest a number of different behaviors based on the rheologic structure prior to folding. Where a strong upper crust overlies a weak lower crust and mantle, as in very young lithosphere, folds develop along the top and bottom of the upper crust monoharmonically (Fig. 4.19a). If the upper mantle is strong, the folds in the upper crust may develop independently from the folds at the top of the upper mantle, producing a decoupled, biharmonic pattern (Fig. 4.19b). The short wave-

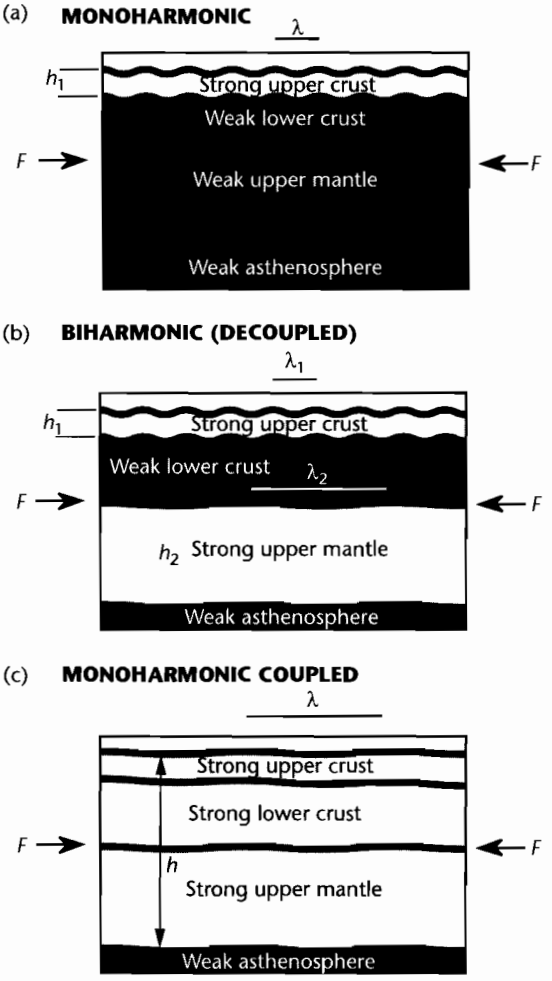

Fig. 4.19 Different styles of periodic buckling by a compressional force F; h_1 and h_2 are the thicknesses of the competent crust and mantle respectively, which fold with wavelengths λ_1 and λ_2. Where the lower crust is very weak, the upper crust and mantle lithosphere fold with different wavelengths ($\lambda_1 < \lambda_2$), producing decoupled or biharmonic folding (b). Where there is a single coherent layer of coupled crust and mantle, as in both young (<150 Ma) and very old (>1000 Ma) lithospheres, monoharmonic folding develops (a) and (c). After Burov et al. (1993) and Cloetingh et al. (1999).

length (30–60 km) corresponds to crustal folds, whereas the longer wavelength (200–350 km) corresponds to mantle folds. Where the combined crust and upper mantle are strong and mechanically welded, as in very old lithosphere, monoharmonic folds once again develop, but with a greater wavelength (>500 km) than in the "young lithosphere" case (Fig. 4.19c).

2 *Irregular or aperiodic folding* generally occurs in very young, weak lithosphere, where the deformation is strongly affected by such factors as erosion, lateral spreading of the sedimentary basin-fill, inhomogeneities in the crust (such as pre-existing sedimentary basins), and nonlinear rheologic behavior. Both wavelengths and amplitudes may vary unsystematically along the plate. They may also vary with progressive shortening.

Based on numerical plane strain models using nonlinear elastic–plastic (crust) and temperature-dependent power-law creep, Burg and Podladchikov (2000) predicted that lithospheric buckles, flanked by sedimentary basins, should spontaneously evolve into regions of asymmetric folding and thrusting. For example, the Kashmir and Peshawar basins either side of the Hazara–Kashmir syntaxis in northern Pakistan are thought to have been initiated by buckling. The Miocene to Recent central and south Adriatic basins, located between the Apennines and the Dinarides of southern Europe, are also thought to be due to lithospheric buckling of the Adriatic crust (Bertotti et al. 2001) (Fig. 4.20).

A persistent problem is how buckles are maintained over geological time scales, since in the absence of continuing compression, they should collapse because of the density contrasts between crust and mantle at the Moho. Only very strong crustal rheologies, expected in cold, strong cratons such as Australia or the Russian Platform, would be expected to withstand these pressure differences at the Moho for geological time scales of >20 Myr. In weak lithospheres, the buckles may collapse within 10 Myr.

Since basins due to lithospheric buckling are likely to be found in the foreland of continental collision zones, they may be difficult to discriminate from flexural basins driven by essentially vertically applied load systems in mountains belts. Despite some similarities in wavelength and amplitude, the main discriminating factors between the two types of basin are:

- Flexural foreland basins are very deep (< 10 km) close to the thrust front and taper strongly towards the foreland. Beyond the flexural forebulge in the backbulge region, amplitudes of the deflection are very small ($\ll$200 m). Migration of the orogenic wedge causes major stratigraphic onlap of the foreland plate through time;
- basins due to lithospheric buckling appear to form within a train of uplifts and depressions extending for $\gg$1000 km from the plate boundary. Depressions may be 10^2–10^3 m deep, with sediment derived from both margins, producing a symmetrical stratigraphic stacking.

Flexural foredeeps and basins due to lithospheric buckling should therefore not be confused. However, it may be very difficult to discriminate between some backbulge depositional zones and some basins representing synforms due to lithospheric buckling.

4.5 THE DYNAMICS OF OROGENIC WEDGES

4.5.1 Introduction

Foreland basins are dynamically linked to associated orogenic belts. The evolution of the orogenic wedge is important for basin development in a number of ways: (i) The wedge represents a supracrustal load on the foreland plate: its geometry and structure therefore influence the deflection of the foreland plate, (ii) the shortening and thickening of the wedge, or its extension and forward propagation, change the *configuration* of the load with respect to the deflected plate, i.e., its magnitude and distribution over the deflected plate, and thus change the shape of the deflection, and (iii) the unroofing by tectonic uplift and erosion of the orogenic wedge provides the detritus for deposition in the basin.

Here we concentrate on some of the broad processes of orogenic wedge evolution that have some bearing on the deflection of the foreland plate. Further information on foreland basin stratigraphy can be found in §8.6.2.

Three possible mechanisms for the driving forces responsible for crustal shortening have been proposed: (i) *gravity sliding*, (ii) *gravity spreading*, and (iii) *horizontal deviatoric push*. Gravity sliding requires a potential energy gradient for sliding under gravity alone. The gravitational force acting on the gradient must overcome the resistance to movement for gravity sliding to occur. Mathematical models suggest that the angle need only be small (a few degrees) where the effective normal stress on the inclined surface is reduced by the presence of high pore fluid pressures (Hubbert and Rubey 1959). However, field studies, particularly in the Rocky Mountains (e.g., Dahlstrom

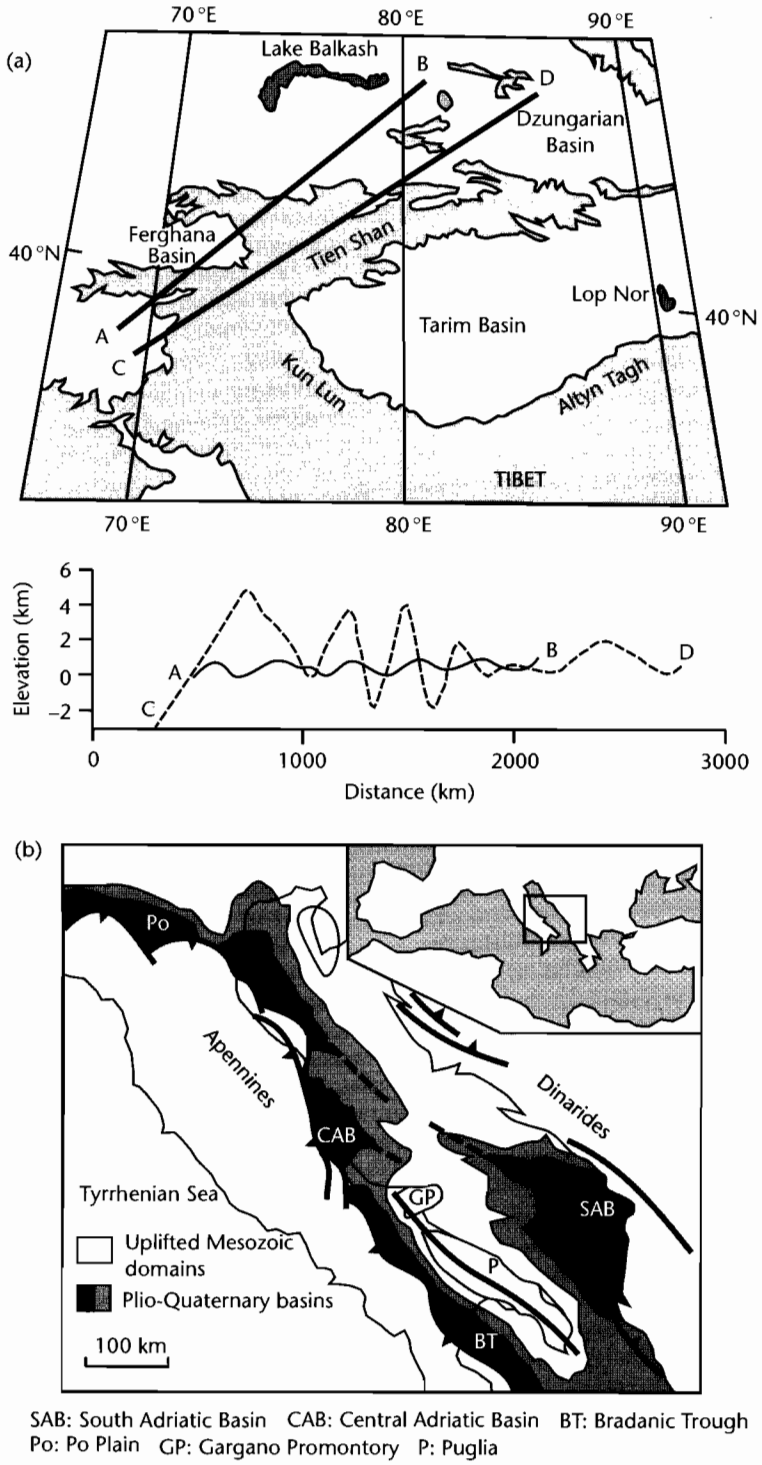

Fig. 4.20 Real-world examples of buckling from (a) central Asia (Cloetingh et al. 1999), showing elavation profiles for two transects A–B and C–D, and (b) Adriatic and eastern Italy (Bertotti et al. 2001), showing basins and highs oriented parallel to the strike of the Apennines and Dinarides. Reproduced courtesy of American Geophysical Union.

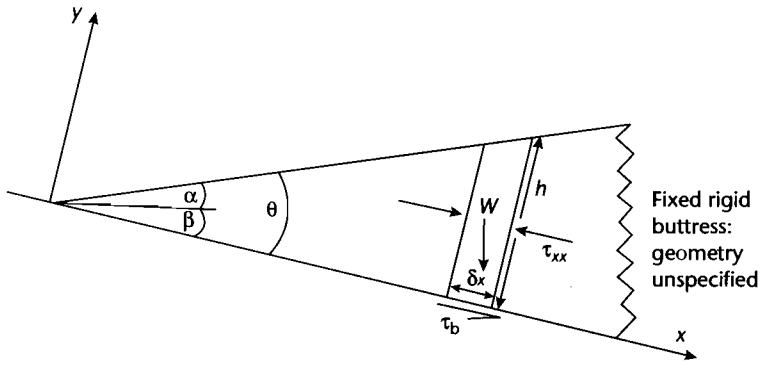

Fig. 4.21 Simplified model of an accretionary wedge (after Platt 1986). α is the surface slope, β is the basal slope and θ is the taper angle ($\alpha + \beta$). A small segment of the wedge of basal length δx and height h is subjected to a body force W, to a basal traction $\tau \delta x$, and to "push" forces from the rear, produced by the longitudinal deviatoric stresses τ_{xx}. The force balance is expressed in equation (4.26). Frontal accretion, underplating, erosion, and changes in basal shear stress (for examples by changes in the rate of convergence/subduction) place the wedge out of equilibrium. The wedge responds by shortening and thickening or by collapsing by extension.

1970) suggest that many thrusts dip in the opposite sense to the mass transport direction. Gravity sliding is therefore not likely to be the sole or dominant process in mountain belt tectonics. In the discussion that follows, we therefore concentrate on models involving horizontal deviatoric push and gravitational spreading. The most commonly used model involves a force balance in a tapered orogenic wedge.

4.5.2 Critical taper theory

Price (1973) believed that orogenic wedges behave as plastic entities as a result of the interfingering of a large number of thrust sheets into a mechanically interdependent system. Gravity acting on an orogenic "high" would provide the driving force for a spreading along thrust faults. The horizontal shear stress produced by gravity is given by (Elliott 1976)

$$\tau = \rho g h \alpha \qquad (4.25)$$

where ρ = density, g = gravitational acceleration, h = depth below surface, and α = surface slope of wedge. However, although this strain system is capable of producing local shortening, which must be compensated elsewhere by extension in order to maintain a constant angle of the wedge, it cannot explain the evidence of large scale net shortening in orogenic belts. Nor is any explanation given for the prior existence of a gravitational "high" at the onset of spreading.

Horizontal compressional forces (deviatoric "pushes") exerted along convergent plate boundaries may be primarily responsible for the dynamics of orogenic wedges. The convergent orogen can be regarded as a wedge-shaped prism resting on a rigid slab with a rigid buttress at the rear (Chapple 1978). The wedge behaves as a single mechanically continuous, dynamic unit, with the longitudinal force applied at the rear of the wedge counterbalanced by resistance to sliding on its base. The geometry attained is one of a wedge tapering along its length with a dynamic balance between the gravitational forces arising from the slope of the wedge, the push from the rear and the basal shear force or "traction." This balance can be expressed as follows (Platt 1986).

$$\tau_b = \rho g h \alpha + 2K\theta \qquad (4.26)$$

where the additional term on the right-hand side is due to the horizontal "push," K is the yield strength of the wedge, and θ is the angle at the front of the wedge (Fig. 4.21). Davis et al. (1983) also accounted for the internal strength and pore-fluid pressure of the wedge. They introduced the term "critical taper" to describe the surface slope that would produce a wedge in a state of yield throughout (Fig. 4.21). Davis et al. (1983) therefore expressed the basal shear stress in terms of the gravitational force and the material properties of the wedge as follows:

$$\tau_b = \rho g h \alpha + (1 - \lambda) K \rho g h \theta \quad (4.27)$$

where λ is the ratio of pore-fluid to lithostatic pressure, and the other terms are essentially the same as in equation (4.26).

Platt (1986) predicted patterns of deformation in the orogenic wedge resulting from externally imposed changes in its geometry. The most important change results from accretion. Two types are recognizable:

- *Frontal accretion* is the accumulation of material at the tip of the wedge, thereby lengthening the wedge. The response, if longitudinal deviatoric stresses are large enough, is internal shortening of the wedge. This may take the form of out-of-sequence thrusting or backthrusting;
- *underplating* of material to the underside of the wedge, causing the wedge to thicken and increase in surface slope. The wedge may respond by extension, lengthening the wedge, and lowering surface slopes.

Other factors influencing the shape of the orogenic wedge are: (i) *erosion* or removal of material from the top of the wedge, which encourages renewed shortening, and (ii) *changes in basal shear stress*: an increase in τ_b caused, for example, by an increase in the rate of subduction, leads to shortening and thickening; a decrease in τ_b may cause extension (Dahlen 1984). If subduction ceases, τ_b vanishes and the orogenic wedge should collapse by extension at the rear. Platt (1986) explains the uplift of high pressure rocks to surface positions in the rear of orogenic belts as due to this process of extension (Fig. 4.22).

The implications for basin development of this dynamic model are clear. Variations in rate of subduction, magnitude of deviatoric compression, or material properties of the wedge may cause large temporal variations in the load configuration and therefore in the deflection of the plate. In particular, lengthening and contraction of the wedge will have an impact on the position of the forebulge on the downgoing slab relative to the orogenic front (§4.6.2, §8.3.1).

4.5.2.1 The brittle–ductile transition in critically tapered wedges

The critical taper model is limited to cases of purely brittle-frictional (Coulomb) deformation. Many mountain belts, such as the Andes (Isaaks 1988) and Himalayas (Le Pichon et al. 1992), have a low-gradient toe area, and a steeper slope leading to a broad plateau region. These topographic features can best be explained by using a model including the effects of temperature-dependent ductile creep (Williams et al. 1994) (Fig. 4.23). The basal surface of the wedge, the decollement zone, may have different rheologic properties to the material within the wedge, because of the effects of dynamic crystallization (Rutter and Brodie 1988). This keeps deformation focused on the decollement. At the toe of the wedge, deformation within the wedge and in the basal decollement is dominated by frictional sliding and brittle failure, giving the classic tapered profile. However, at greater depths and higher temperatures the lower part of the wedge becomes ductile. This increases the ratio of applied basal shear stress to the strength of material in the lower part of the wedge, forcing an increase in the taper and a steeper surface slope. At even greater depths, the decollement zone itself may also become ductile, decreasing the ratio of applied basal shear stress to the strength of the lower part of the wedge and causing the surface profile to flatten into a plateau (Fig. 4.23b).

Abrupt changes in the wedge taper and the surface slope are brought about by abrupt changes in either the applied basal shear stress in the decollement zone or by the strength of the material in the lower part of the wedge. Such abrupt changes are most likely caused by a change in the deformational mechanism from brittle to ductile. A model using a brittle–ductile critical taper explains the east–west topographic profile across the Andes (near 20°S) from the Sub-Andean foothills to the steep slopes of the Eastern Cordillera and the high plateau of the Altiplano (Fig. 4.24).

The likelihood of orogenic wedges having brittle–ductile behavior depends on factors such as the thermal environment, material properties of the wedge and decollement materials, convergence rate, and elastic thickness of the lithosphere. Some wedges may be almost perfect frictional Coulomb wedges, such as in Taiwan, whereas others may exhibit significant ductile behavior.

4.5.3 Analogue models

Analogue experiments give insights into the mechanics of crustal deformation in orogenic wedges (Davy and Cobbold 1991). Analogue experiments are scaled to be representative of the lithosphere. Materials are therefore chosen to represent the rheologic layering and strength profile of the lithosphere. A simple system comprises a brittle upper sand layer simulating the crust, and a lower layer of high viscosity power-law silicone representing the lower crust, above a basal low viscosity fluid representing the mantle. This basal fluid layer allows the

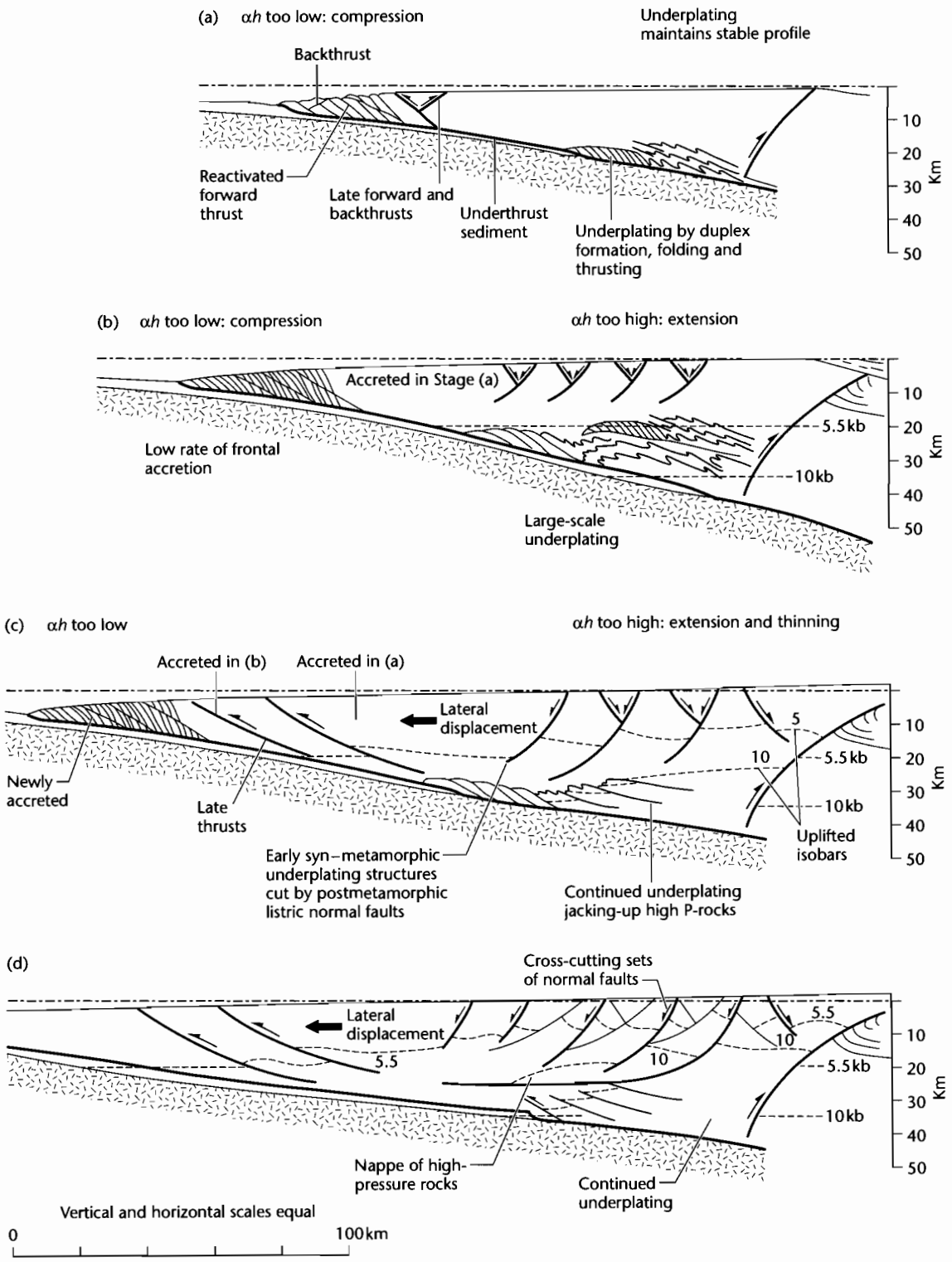
(a) αh too low: compression
Underplating maintains stable profile
Backthrust
Reactivated forward thrust
Late forward and backthrusts
Underthrust sediment
Underplating by duplex formation, folding and thrusting
10
20
30
40
50
Km
(b) αh too low: compression
αh too high: extension
Accreted in Stage (a)
Low rate of frontal accretion
5.5kb
10kb
Large-scale underplating
10
20
30
40
50
Km
(c) αh too low
αh too high: extension and thinning
Accreted in (b)
Accreted in (a)
Lateral displacement
Newly accreted
Late thrusts
Early syn–metamorphic underplating structures cut by postmetamorphic listric normal faults
5
10
5.5kb
10kb
Uplifted isobars
Continued underplating jacking-up high P-rocks
10
20
30
40
50
Km
(d)
Cross-cutting sets of normal faults
Lateral displacement
5.5
10
5.5
10
5.5kb
10kb
Nappe of high-pressure rocks
Continued underplating
Vertical and horizontal scales equal
0
100km
10
20
30
40
50
Km

analogue experiment to be isostatically balanced. In a four-layer system, a brittle upper mantle lithosphere layer and ductile lower mantle lithosphere layer are constructed beneath a brittle upper crust and ductile lower crust.

Shortening in analogue experiments is normally produced by a piston and commonly results in buckling followed by bivergent thrusting (Cobbold et al. 1993; Burg et al. 1994b). The buckles have a wavelength controlled by the relative thicknesses of the brittle and ductile layers. Scaled up to the real world, such large buckles should be obvious as major crustal scale antiforms with a wavelength of *c.* 200 km, such as the Penninic culmination of the central Alps of Europe (Burg et al. 2002). The thrusts originate from the inflection points of the major buckles, and so are controlled in location and spacing by the presence of the early first-order buckles. Further shortening results in amplification of the thrusted buckles, giving rise to imbricated brittle wedges.

Indentation sand box models involve a rigid indenter

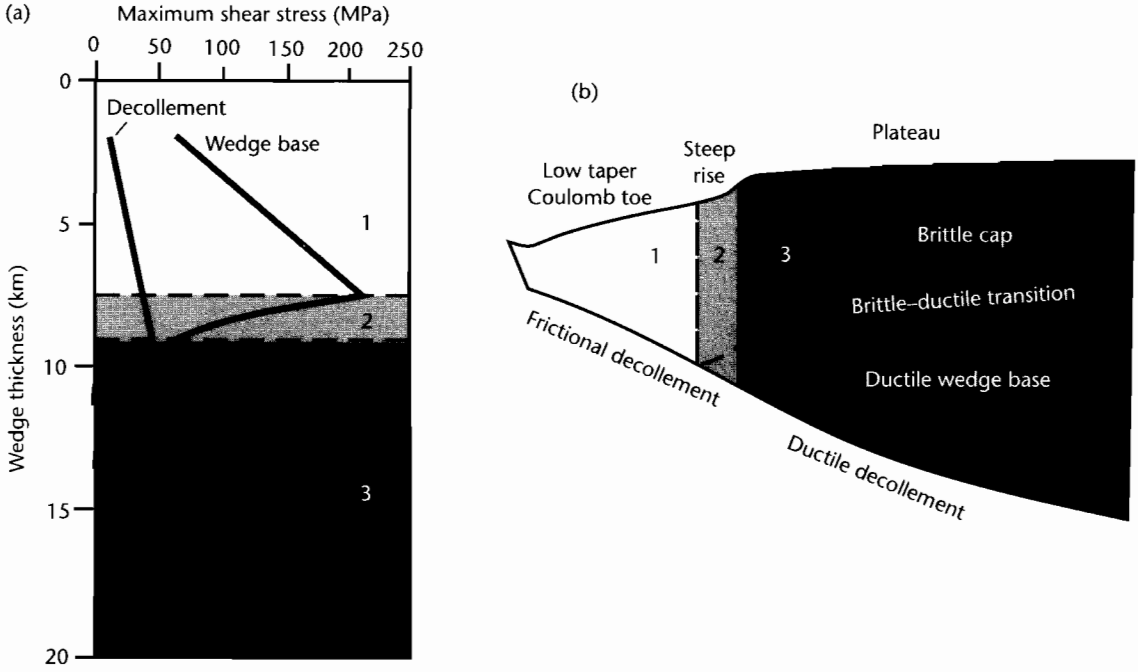

Fig. 4.23 Brittle–ductile critical taper model (after Williams et al. 1994). The wedge is divided into three regions: a narrow taper toe, where both the basal decollement and the wedge base behave in a brittle–frictional manner (Zone 1); a steep rise, where the decollement is still frictional but the wedge base region is ductile (Zone 2); and a flat plateau region, where both the wedge base and the decollement behave in a ductile manner (Zone 3). (a) The maximum shear stress (strength) of the wedge base and decollement; (b) The geometry of a critically tapered wedge corresponding to the strength profiles shown in (a). Reproduced courtesy of American Geophysical Union.

Fig. 4.22 Platt's (1986) evolutionary model of an accretionary wedge from youth to maturity. (a) Early stage with frontal accretion dominant. The gravitational effect of the surface slope (first term on right hand side of equation (4.27)) is too low in the frontal region, which therefore shortens and thickens internally; (b) Large scale underplating is the dominant mode of accretion, so that the rear of the wedge extends by extensional faulting and possibly by ductile flow near the base of the wedge. The deeper parts of the wedge may also undergo high pressure metamorphism; (c) Continued underplating and resultant extension has lifted the high pressure rocks towards the surface. Extension towards the rear of the wedge promotes some shortening (late thrusting) at the front; (d) In the mature stage underplating and extension have brought the high pressure rocks to levels accessible to erosion. The prism is now 300 km long, comparable to the Makran wedge of Pakistan.

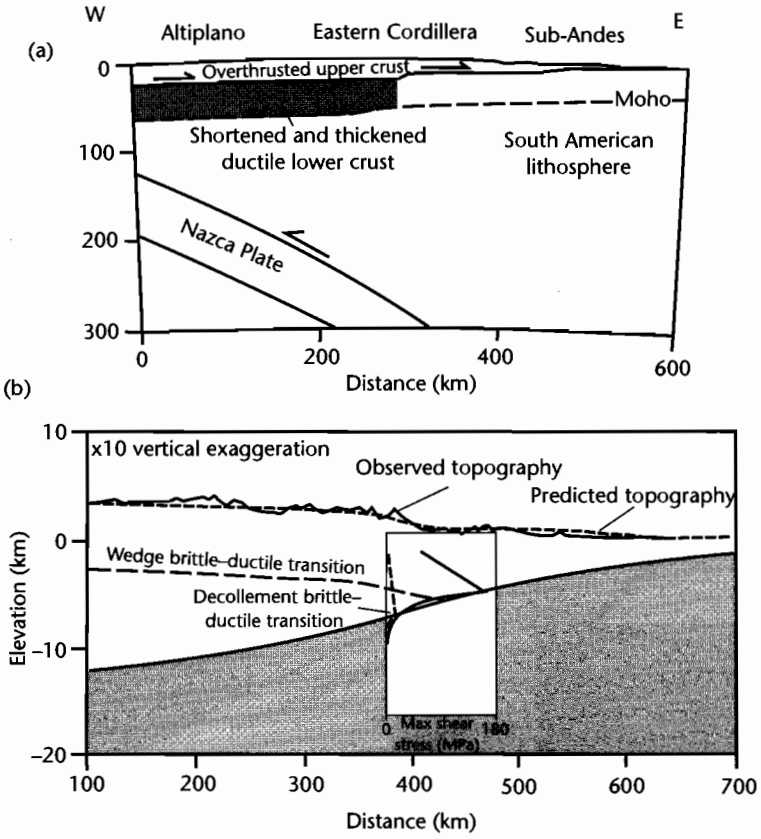

Fig. 4.24 Results of a brittle–ductile critical taper model applied to the Andes at 20 °S (after Williams et al. 1994). (a) Crustal model of the Andes along a transect at 20 °S (after Isacks 1988); (b) Observed and modeled topography using the geometry shown in cross-section, with the strength profile for wedge base (solid line) and decollement (dashed line) superimposed. The wedge base is significantly stronger than the decollement zone, except at where the decollement becomes ductile (*c.* 7.5 km below sea level). Reproduced courtesy of American Geophysical Union.

with the same height as the undisturbed sand (representing undeformed crust), which allows sand to spread laterally outwards over the indenting plate (Koons 1989, 1990). With progressive deformation, a doubly vergent wedge forms, with thrusts propagating away from the indenter to form an outboard wedge or retro-wedge, and towards and over the indenter as an inboard wedge or pro-wedge. The outboard wedge is decoupled along a low-friction Mylar sheet at the base, and thrusts rise from this surface. However, within the inboard wedge, thrusts propagate up through the wedge material itself at an angle corresponding to the angle of internal friction of the sand ϕ. Thrusts in the inboard wedge are therefore shallower than in the outboard wedge. Sand box experiments are also capable of reproducing the conditions of mantle subduction, where a sand cover is dragged by an underlying Mylar sheet (Malavieille 1984). Once again, a doubly vergent wedge is produced centered over the point of detachment, the majority of thrusts facing the subducting plate.

Analogue experiments are therefore good at allowing a visualization of the development of major crustal features such as thrusted antiforms and bivergent wedges. The tectonic wedges created in analogue experiments have geometries as predicted by critically tapered wedge mechanics (§4.5.2) and are very similar to the wedges produced in numerical simulations using the same boundary conditions (see §4.5.4 and §4.6.3). However, they have difficulty in simulating erosion at the surface of the wedge.

4.5.4 Numerical approaches to orogenic wedge development

There are three force systems that control deformation in the orogenic wedge:

- **F1**: The compressive force integrated over the thickness of the crust;
- **F2**: the gravitational force (or increased potential energy) due to crustal thickening;
- **F3**: the basal traction force integrated across the base of the deforming zone.

The tendency for the thickened crust to spread out laterally is given by the ratio **F2/F1**, which is known as the *Argand number* (see also §3.6.2) (England and McKenzie 1982). For a linear viscous material

$$Ar = \frac{\rho g h^2}{\mu V_p} \tag{4.28}$$

where ρ is the density, g is acceleration of gravity, μ is viscosity, h is the length scale (thickness) of the mechanical model, and V_p is the horizontal velocity at the base of the crust. For a typical crust with $\rho = 2800\,\mathrm{kg\,m^{-3}}$, $\mu = 10^{23}$ Pa s, $h = 35\,\mathrm{km}$, and $V_p = 0.05\,\mathrm{m\,yr^{-1}}$, the "viscous" Argand number is 5. For a Coulomb plastic material, the Argand number becomes (Willett 1999)

$$Ar = \frac{2}{\tan\phi} \tag{4.29}$$

where ϕ is the angle of internal friction, typically 15° for crustal rocks. Using this value, the "Coulomb" Argand number is 7.

If $Ar \gg 1$, even small increases in thickness are counteracted by gravity, redistributing the thickening away from the plate boundary and broadening the zone of deformation. If Ar is small, however, the crustal thickening is localized.

The ratio **F3/F1** is known as the *Ampferer number* (Ellis et al. 1995; Ellis 1996). It reflects the strength of the crust–mantle coupling. The length scale of deformation in subduction models scales on the Ampferer number. If Am is nearly 1, the model crust is strongly coupled to the underlying mantle, which means that the basal tractive forces are transmitted strongly into the crust, causing thickening. If Am is close to zero, there is weak coupling, and the basal tractive forces are inefficient at causing crustal thickening.

Numerical models of orogenic wedge development have been developed from two starting points (Fig. 4.25a):

1 *Indentation models* assume that forces are transmitted laterally from a rigid indenter into a less rigid continental plate approximated by a thin viscous sheet (England et al. 1985; England and Houseman 1986). As mimicked by plasticine analogue models (e.g., Peltzer and Tapponnier 1988), deformation of the viscous sheet spreads out over a strike-normal distance related to the width of the indenter. If λ is the length scale of the deformation and D is the strike-parallel width of the indenting body

$$\lambda = \frac{2D}{\pi\sqrt{n}} \tag{4.30}$$

where n is the power-law exponent of the viscous sheet. In this model, if D is 3000 km, which is the approximate scale of the India–Asia collision, and the rheology of the viscous sheet is linear ($n = 1$), the length scale of the deformation should be in the region of 2000 km. For $n = 2$ and n = 3, λ reduces to 1350 km and 1100 km respectively. In the indentation model, crust (and mantle lithosphere) is thickened in the relatively weak continental lithosphere against the boundary with the rigid indenter. Gravity acts on the thickened layer, which causes λ to increase as convergence continues. Eventually, very large regions of crustal uplift such as the Tibetan Plateau are produced. The forces on the thickened crust are quantified by the Argand number in indentation models.

2 *Mantle subduction* models invoke the transmission of forces from an underlying subducting mantle lithosphere to the base of the crust. These forces act across a crust–mantle boundary that must therefore undergo considerable subhorizontal shear. This zone of subhorizontal decoupling is termed a *detachment*. The width of the region of crustal thickening depends critically on the strength of the coupling along the detachment. This coupling is quantified by the Ampferer number. If the original thickness of the crust is h_0, the length scale of the deformation in mantle subduction models is given by

$$\lambda = \left(\frac{4}{nAm}\right)^{\frac{n}{n+1}} h_0 \tag{4.31}$$

If the crustal layer is initially 35 km thick, we adopt a linear viscous rheology ($n = 1$) and a very strong coupling between the crust and mantle ($Am = 1$), the width of deformation is just 70 km. If there is a very weak coupling between crust and mantle ($Am = 0.1$), λ becomes *c.* 220 km. Both of these estimates are considerably

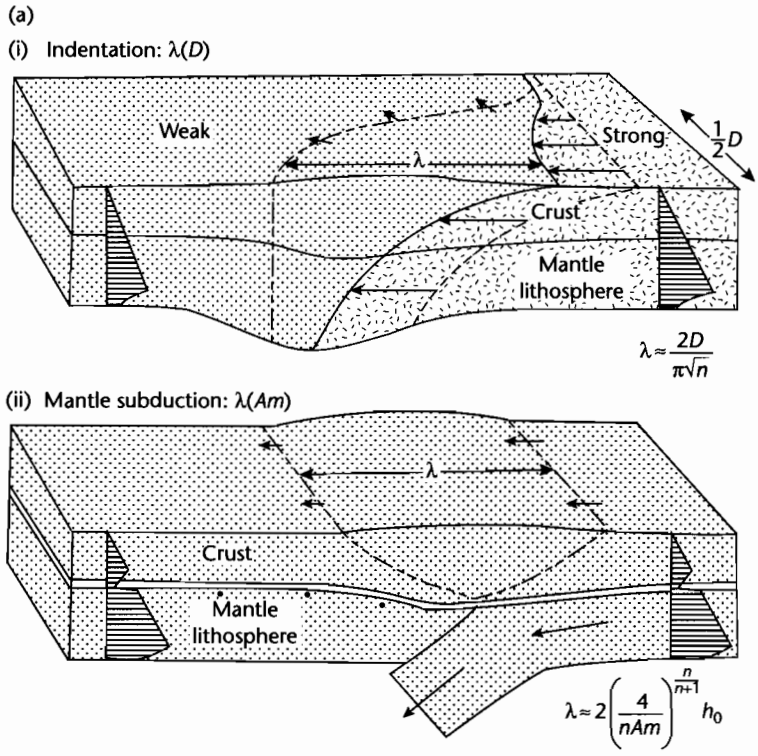

Fig. 4.25 (a) Schematic illustration of two end-member models of continental deformation resulting from convergent continent–continent tectonics (after Ellis 1996). In (i), indentation over a lateral length scale D causes thickening over a width λ. Half of the indenter is shown. Thickening occurs in the crust and mantle lithosphere in the relatively weak indented plate. (ii) Continental deformation is driven mostly by mantle subduction. Crust in both plates is weak, with a strength minimum at the Moho, which decouples crustal deformation from underlying mantle subduction. The width of deformation λ depends on the strength of the mantle–crust coupling, given by the Ampferer number Am; (b) Deformation width λ normalized by the initial crustal thickness h_0, versus the crust–mantle coupling Am. The normalized indenter lateral length scale is $D/h_0 = 25$. For a given indenter length scale, the combined model width of deformation width λ is controlled by indenter mechanics for weakly coupled (detached) systems ($Am = 0$), and by mantle subduction mechanics for strongly coupled ($Am \sim 1$) systems. Reproduced courtesy of Geological Society of America.

smaller than in the indentation model, suggesting that the length scale of deformation in an orogenic belt is an indicator of the underlying mechanics.

Comparing the indentation and mantle subduction models (Ellis 1996), the increase in the width of deformation increases with continued convergence, but at different rates. The value of λ is initially much lower in the mantle subduction case, but the growth of λ with convergence increases more rapidly than in the indentation model (Fig. 4.25b).

An orogenic model involving both indentation and mantle subduction processes suggests that there may be different evolutionary paths for orogenic belts:

1 For situations where the crust is strongly coupled to the mantle lithosphere (Am high) crustal thickening should initially be controlled by mantle subduction, especially where D is large. In the case of orthogonal relative plate motion, there will be very limited strike–slip or escape tectonics;
2 for situations where the crust is weakly coupled to the mantle lithosphere (Am low), mechanics will be dominated by indentation, especially for small indenter length scales (D). Even during orthogonal convergence, strike–slip tectonics and lateral escape should be widespread;
3 since λ grows faster for mantle subduction than for indentation, an orogen initially dominated by mantle

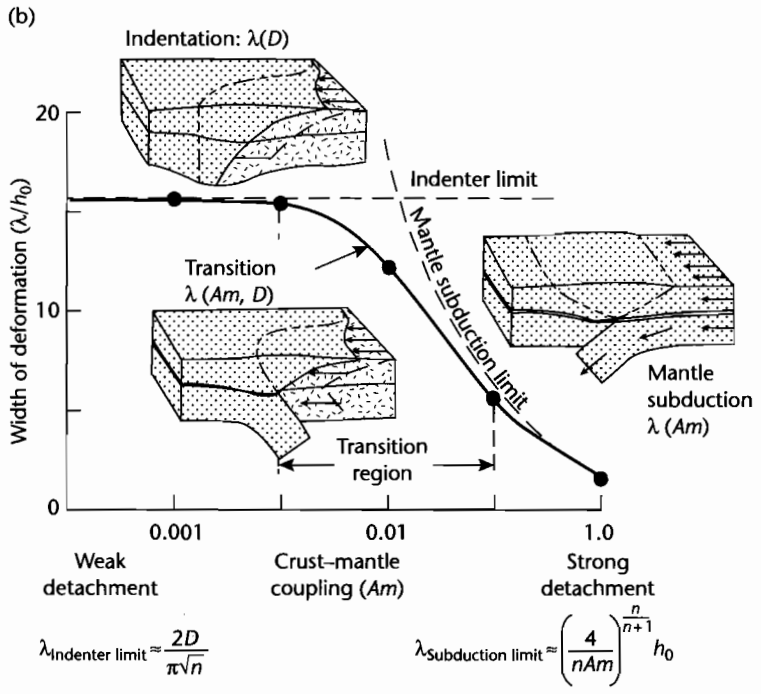

Fig. 4.25 *Continued*

subduction mechanics may, with continued convergence, evolve into an orogen dominated by indenter-style mechanics.

4.5.4.1 The mechanics of bivergent wedges

We have so far considered the mechanics of critically tapered orogenic wedges as a Coulomb model (Davis et al. 1983; Dahlen 1984; Platt 1986) and that the gross features of convergent orogens can be simulated from analogue experiments (Malavieille 1984). One of the conspicuous features of mountain belts and oceanic accretionary prisms is their doubly vergent nature. That is, thrust displacements are directed outwards from the core of the orogen on both flanks. Bivergent wedges can also be produced in numerical experiments involving the subduction of mantle lithosphere beneath a crustal layer with a Coulomb-plastic rheology (Willett 1992; Beaumont et al. 1996a). The basic model set up is a laterally uniform layer undergoing a plane strain deformation caused by coupling across a detachment to two underlying, converging rigid plates. One underlying plate slides (subducts) beneath the other at point *S*. At the base of the upper layer, the velocity field to the left of *S* is uniform and positive, acting from left to right (Fig. 4.26), whereas to the right of *S* the velocity is zero. The upper layer has a Coulomb yield strength with a coefficient of friction ϕ that is larger than the coefficient of friction in the weak detachment layer ϕ_d. Model runs show that deformation spreads upwards from *S*, initially as two conjugate shear zones, bounding a nearly triangular region of minimal internal deformation that is uplifted as a block (Fig. 4.27a). Subsequently, shear zones develop on the pro-wedge side of *S*, producing a long, tapered pro-wedge compared to the narrow retro-wedge (Fig. 4.27b). Finally, the retro-wedge is detached from its base and propagates strongly to the upper plate, producing a tapered retro-wedge (Fig. 4.27c). Whereas the pro-wedge grows by accretion at its toe and has the minimum taper angle for a critically tapered Coulomb wedge, the retro-wedge grows by material being added at the back, and has the maximum taper for a critically tapered Coulomb wedge. This is supported by the obviously different topographic slopes on the different flanks of mountains belts such as the Southern Alps of New Zealand and Alps of central–western Europe.

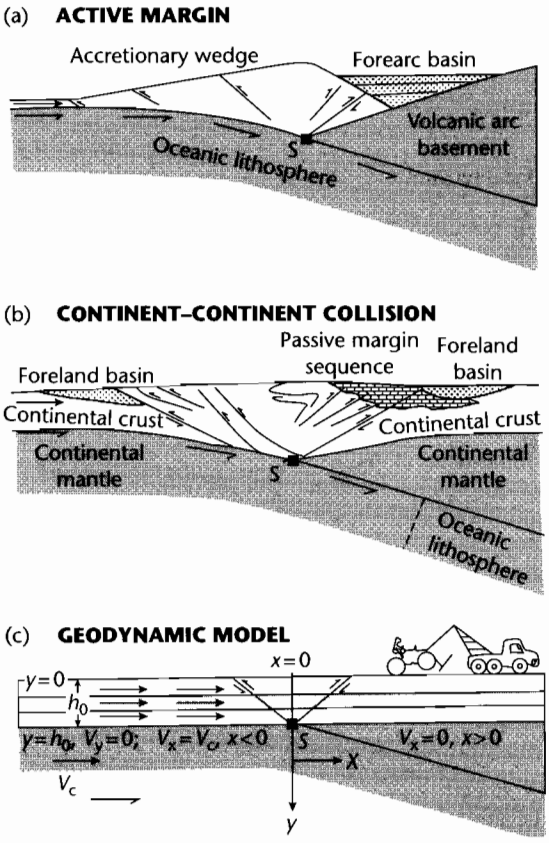

Fig. 4.26 (a) Active margin with bivergent wedge represented by an accretionary prism and a retro-basin represented by a forearc basin, and a pro-basin as an ocean trench; (b) Continent–continent collision zone with a pro-foreland and retro-foreland basin; (c) Geodynamic model, showing crustal deformation focused at a point S, where mantle of the plate on the left, moving with a constant tangential velocity V_p detaches and is underthrusted. Overlying crust has initial thickness h_0 to the left of S. The tangential velocity to the right of S is zero. There is no stress on the upper surface. There is no requirement for a "bulldozer" backstop in this geodynamic model. Modified from Willett et al. (1993). Reproduced courtesy of Geological Society of America.

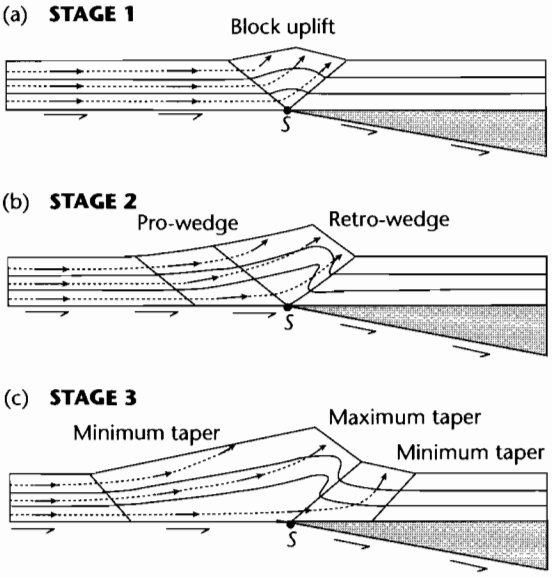

Fig. 4.27 Evolutionary development of a bivergent wedge (from Willett et al. 1993) from a block uplift bounded by two conjugate shear zones centered over S (a), to an asymmetrical bivergent wedge (b), and a tapered retro-wedge as deformation propagates strongly into the upper plate (c). Dashed lines are instantaneous flow lines with arrows proportional to velocity. Reproduced courtesy of Geological Society of America.

The thickened upper layer must be balanced isostatically, giving a crustal root. If the orogen is supported flexurally, flanking foreland basins will develop. As the root develops, however, heating may cause the rheology of crustal materials to change from a Coulomb-plastic flow to a thermally-activated power-law viscous flow (Fig. 4.28). This weakens support for the orogenic wedge, promoting the development of low surface slopes bounding a plateau. If heating continues, the orogen may collapse by extension in order to achieve a low taper angle. Orogenic collapse (Dewey 1988) drives material to the flanks, which continue to behave as Coulomb-plastic wedges. Consequently, extension in the rear of an orogen should be accompanied by contraction (thrusting) towards the flanks. The requirement of the wedge to alter its taper angle also depends on the convergence velocity. If the convergence velocity falls, the viscous-based orogen is required to achieve a new geometry with a lower taper, which can best be achieved by extension. If the convergence velocity stops, the wedge must extend until there is no surface slope. The removal of material from the surface of the wedge by erosion has a strong feedback to the generation of mass in the orogenic wedge caused by convergence. We should expect high rates of erosion to require high tectonic fluxes into the wedge to replace the material lost at the surface (Fig. 4.29). Consequently, erosion appears to "suck up" rocks from depth. This can be recognized in the exhumation patterns of mountain

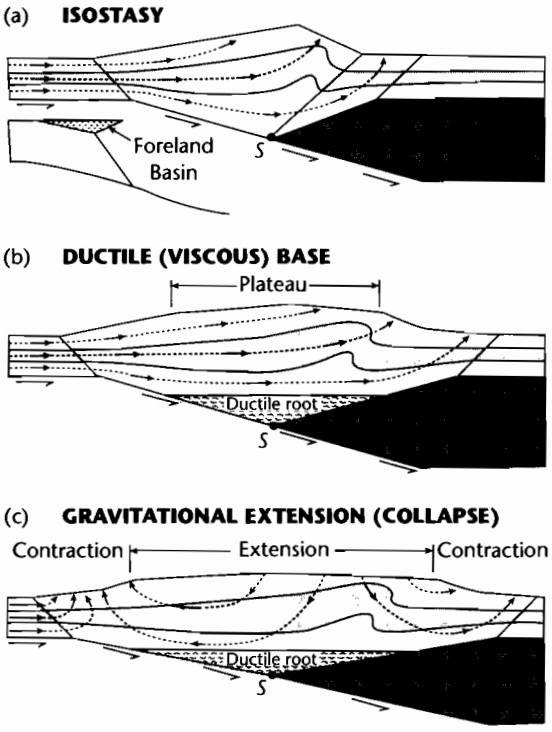

Fig. 4.28 The effects of isostasy and viscous (ductile) flow in the lower crust beneath a bivergent wedge (after Willett et al. 1993). In (a), isostasy causes the formation of flexural depressions (foreland basins); (b) Thickening of the bivergent wedge and increase in temperature decreases basal strength of the wedge and produces a ductile root. This promotes a reduction of surface slopes, resulting in a broad plateau. In (c), a further increase in lower crustal temperatures, or a decrease in the convergence rate causes the plateau to extend and increases contractional deformation in the bounding pro- and retro-wedges. Reproduced courtesy of Geological Society of America.

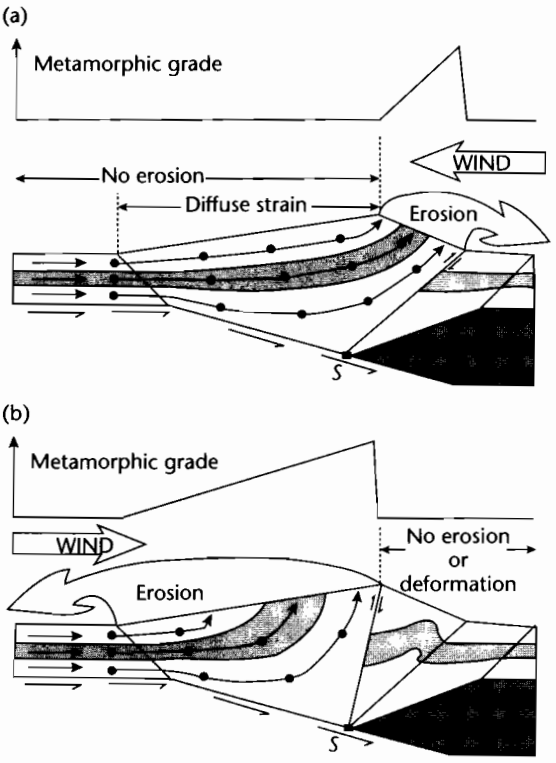

Fig. 4.29 Effects of erosion on a bivergent wedge (after Willett et al. 1993). Precipitation concentrated on the retro-wedge (a), and pro-wedge (b) increases erosion, causing an advection of high-grade metamorphic rocks from the middle and lower crust (and even mantle lithosphere) to the surface. Passive shaded layer shows middle crust. Lines are material trajectories and dots show progressive equal-time positions of points originally aligned vertically. Reproduced courtesy of Geological Society of America.

belts, which commonly have lower crustal (and even mantle) rocks exposed in their cores. If erosion is asymmetrical because of climatic differences on each side of the mountain belt, the wet, windward side of the orogen should be characterized by high exhumation rates of high grade metamorphic rocks, whereas the dry leeward side should continue to be draped by upper crustal rocks (Fig. 4.29). This pattern is seen well in the Southern Alps of New Zealand (Koons 1989; Norris et al. 1990), the central Himalaya (Fielding 2000), the European Alps (Beaumont et al. 1996a; Schlunegger and Willett 1999), and Taiwan (Lin 2000; Dadson et al. 2003).

We reconsider these scenarios posed by numerical models in relation to exhumation, sediment flux, and basin development in §4.6.3.

4.6 THE MODELING OF FORELAND BASINS

4.6.1 Basin evolution caused by a moving tectonic load

Deposition in foreland basin systems can be understood by investigating the effects of a moving load system on the deflection of an elastic foreland plate (Jordan 1981, and Schedl and Wiltschko 1984 for early treatments).

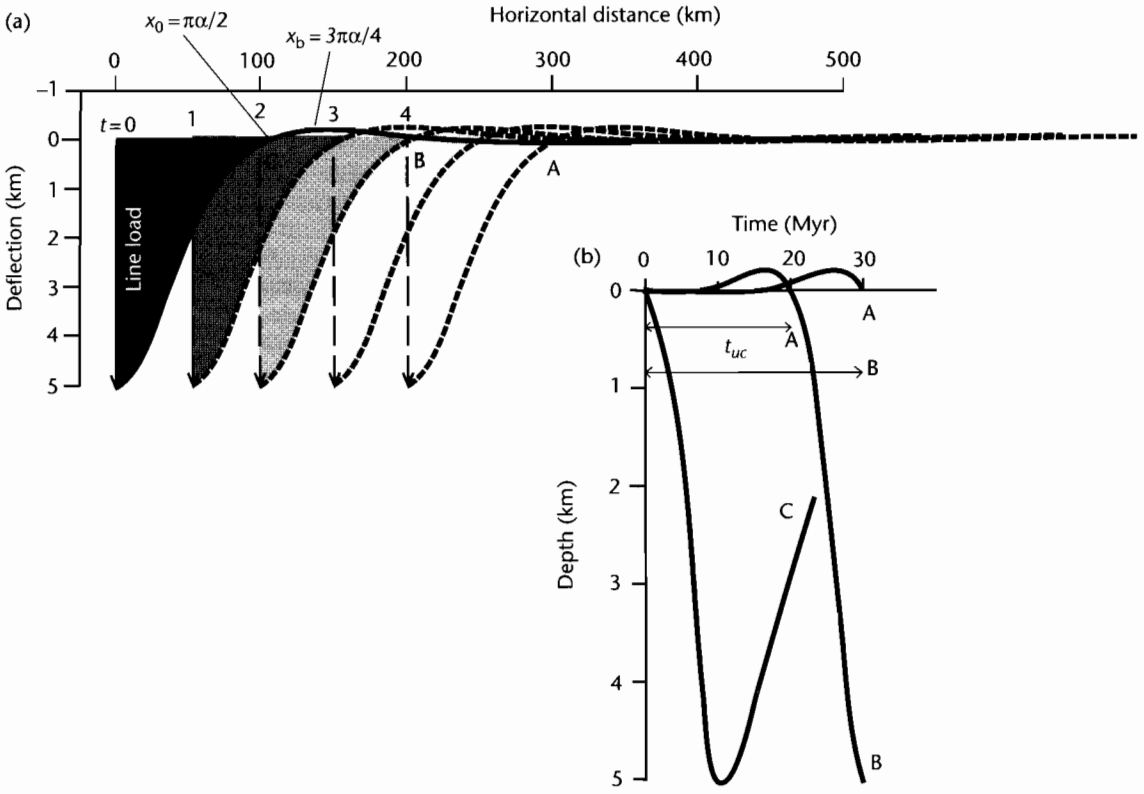

Fig. 4.30 Migration of a flexural wave under a moving load system. (a) Movement of the deflection across a foreland plate as a result of load migration; (b) Points A, B, and C experience different subsidence histories depending on their initial location with respect to the load. Point A spends 30 Myr in a backbulge or forebulge position. Point B is initially uplifted in the forebulge, then subsides in the foreland basin. Point C experiences basin subsidence, followed by uplift as it is incorporated into the thrust wedge.

The static deflection is described for continuous and broken plate models in §4.2. For a moving load system, the deflection simply moves as a wave through the foreland plate ahead of the load system. If the load system moves relative to the foreland plate, so does the deflection.

The shape of the deflection is an asymmetric "low" (foredeep) close to the load and a broad, low-amplitude, uplifted forebulge far from the load. Since the supracrustal load in a convergent mountain belt moves closer to a point fixed to the foreland plate through time, and since we know from the solution of the flexural equation (eqns 4.4 and 4.8 for continuous and broken plates) that the deflection increases towards the load, it follows that subsidence rates in the foreland basin should accelerate through time, until the same fixed point is overridden by the thrust wedge and sedimentation ceases. The original location of the point fixed to the foreland plate at the onset of flexure determines the precise subsidence history followed (Allen et al. 1991). Consider the following three locations (Fig. 4.30):

1 *Point A* is originally located beyond the flexural forebulge in the backbulge region (i.e., for a line load on the end of a broken plate, at $x/\alpha > 5$). It will initially experience negligible uplift/subsidence, but as convergence continues, will be "dragged" through the flexural forebulge, causing slow but prolonged rock uplift and erosion. The erosion will continue until $x = \pi\alpha/2$, producing an unconformity with a large chronostratigraphic gap of duration t_{uc};
2 *Point B* is originally situated within the forebulge region ($\pi\alpha/2 < x < 3\pi\alpha/2$). It will immediately experience

rock uplift and erosion. As convergence continues it will be dragged through the first node of the deflection where $w = 0$, and will then experience accelerating subsidence as the point becomes buried by foreland basin sediments. The chronostratigraphic gap should be smaller than for Point A;

3 *Point C* is originally located close to the orogenic wedge inboard from the first node and the flexural bulge. It will, from the outset, experience subsidence. The rate of subsidence will increase through time as the point becomes closer to the maximum deflection. Eventually, with continued convergence, the point is likely to become incorporated into the orogenic wedge itself so that the foreland basin stratigraphy can only be viewed in allochthonous thrust units. There should be a conformity at the basal surface of the foreland basin megasequence.

The key prediction for a foreland basin generated by a moving load is therefore that the basin-fill is underlain by an unconformity with a variable and predictable stratigraphic gap (Crampton and Allen 1995; Allen et al. 2001). This is a megasequence boundary caused by flexural forebulge uplift. Points located close to the load start subsiding earlier than distal points. At any one time slice, proximal locations subside faster than distal locations. The overall form of the subsidence rate at any one location is convex-up, indicating accelerating subsidence through time (e.g., Homewood et al. 1986). Further discussion is found in §8.3.1.

The plate tectonic scenario providing the context for the general evolution of foreland basins involves the inheritance of a passive margin, followed by an early convergent stage characterized by deep water conditions, and a later convergent stage during which a subaerial wedge is flanked with terrestrial or shallow marine foreland basins (see also §8.3.1) (Stockmal et al. 1986) (Fig. 4.31). Flexural forebulge unconformities are thought to be best developed during the early convergent stage, but may be buried beneath terrestrial sediments during the late convergent stage (Crampton and Allen 1995).

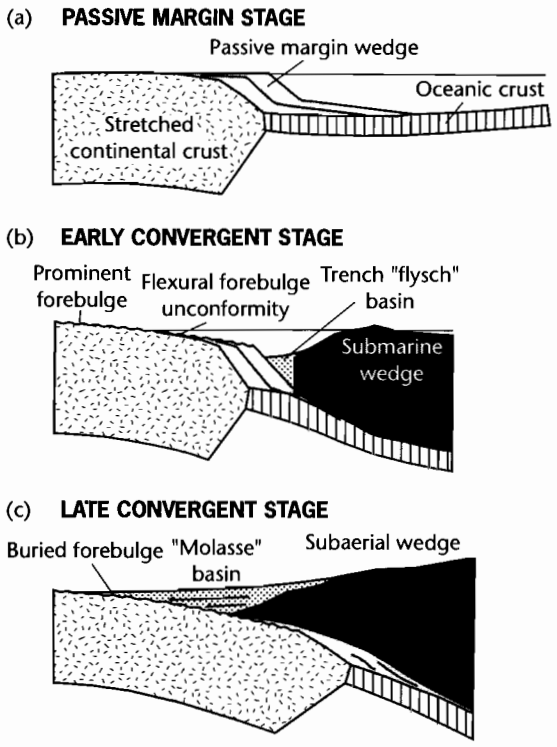

Fig. 4.31 Model involving orogenic loading of a previously stretched continental margin during the early stages of convergence (Stockmal et al. 1986; Watts 1992), modified by Allen et al. (1991). The first orogenic loads are emplaced on a weaker lithosphere at considerable water depths.

4.6.2 Diffusive models of erosion and deposition

The convergence of an orogenic thrust wedge over a foreland plate can be considered mechanically as a distributed vertical load system translating laterally over a flexed plate. Erosion of the thrust wedge and deposition in the foreland basin has been treated as a diffusional process (Flemings and Jordan 1989; Sinclair et al. 1991). In diffusional problems, the transport rate or flux is proportional to the topographic gradient and the rate of erosion or sedimentation is proportional to the curvature. The use of diffusion in modeling hillslope evolution is treated in more detail in §7.5.1.

Sinclair et al. (1991) proposed that the simplest model of mountain belt erosion and foreland basin sedimentation must be described by four parameters (Fig. 4.32): (i) the equivalent elastic thickness of the foreland plate, (ii) the rate of thrust front advance, (iii) the surface slope angle of the orogenic wedge, and (iv) the effective transport coefficient, representing the constant of proportionality between topographic slope and sediment transport rate. They modeled the orogenic wedge as a critically taped system (Davis et al. 1983; Platt 1986; Boyer 1995)

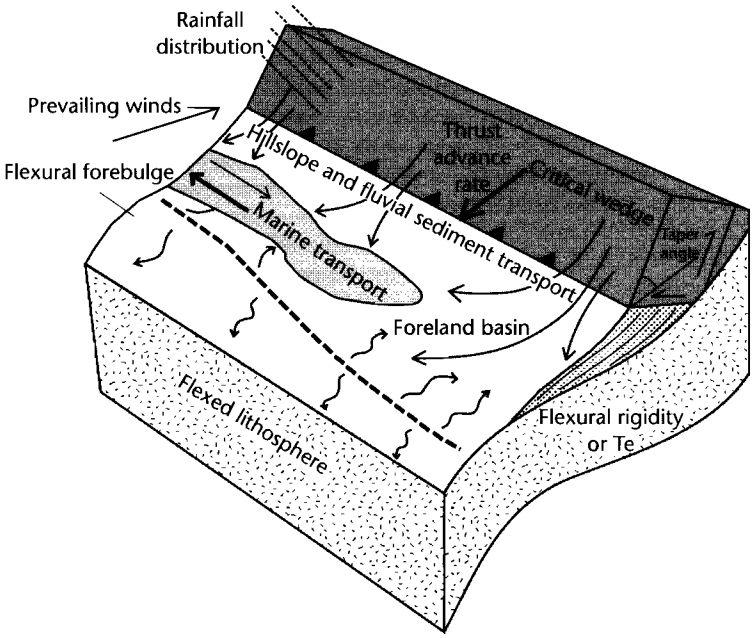

Fig. 4.32 Parameters necessary to describe a diffusive mountain belt system are the advance rate and taper of the orogenic wedge, flexural rigidity of the foreland plate, and sediment transport coefficients. The distinction between relatively local transport on hillslopes and far-field transport in river systems can either be tackled by attributing two different effective diffusivities to these geomorphic subsystems, or by treating the fluvial transport as advective (Johnson and Beaumont 1995).

migrating over an elastic plate that flexurally supports tectonic and sedimentary loads.

From the theory of diffusion, the rate of erosion in the mountain belt or rate of deposition in the basin is given by

$$\frac{\partial h}{\partial t} = K\frac{\partial^2 h}{\partial x^2} \tag{4.32}$$

where K is the effective transport coefficient or diffusivity. Deposition takes place (positive $\partial h/\partial t$) where the topographic curvature ($\partial^2 h/\partial x^2$) is positive. Erosion takes place (negative $\partial h/\partial t$) where topographic curvature ($\partial^2 h/\partial x^2$) is negative. In each increment of time, the thrust wedge moves over the foreland plate, so the total change in distributed load is made of two components

$$\Delta q(x) = \left(\frac{\partial h}{\partial t} + \frac{\partial T}{\partial t}\right)g\rho, \tag{4.33}$$

where the first partial derivative is the topographic change due to erosion or deposition, and the second partial derivative is the change in the tectonic load $T(x)$ in that time step. The new deflection is calculated using flexural isostasy (§2.3.3).

A sensitivity analysis of the four parameters shows that the flexural rigidity of the foreland plate is a first order control on the geometry of the flexed plate and foreland basin, as expected from line-load approximations (§4.2) (Fig. 4.33). However, a greater effect is caused by large variations in the transport coefficient K. For the same flexural rigidity, small transport coefficients ($100\,m^2\,yr^{-1}$) result in narrow, marine basins, whereas high transport coefficients ($800\,m^2\,yr^{-1}$) result in broad, terrestrial basins. The effect of large sediment loads is to force the flexural forebulge far from the orogenic wedge, perhaps even burying it in sediment derived from the orogenic wedge.

Diffusional models have been particularly informative in showing the stratigraphic consequences of changes in the load configuration. For example, a slowing of the advance rate of the orogenic wedge combined with an increase in its surface taper angle, was interpreted by Sinclair et al. (1991) as the cause of distal unconformi-

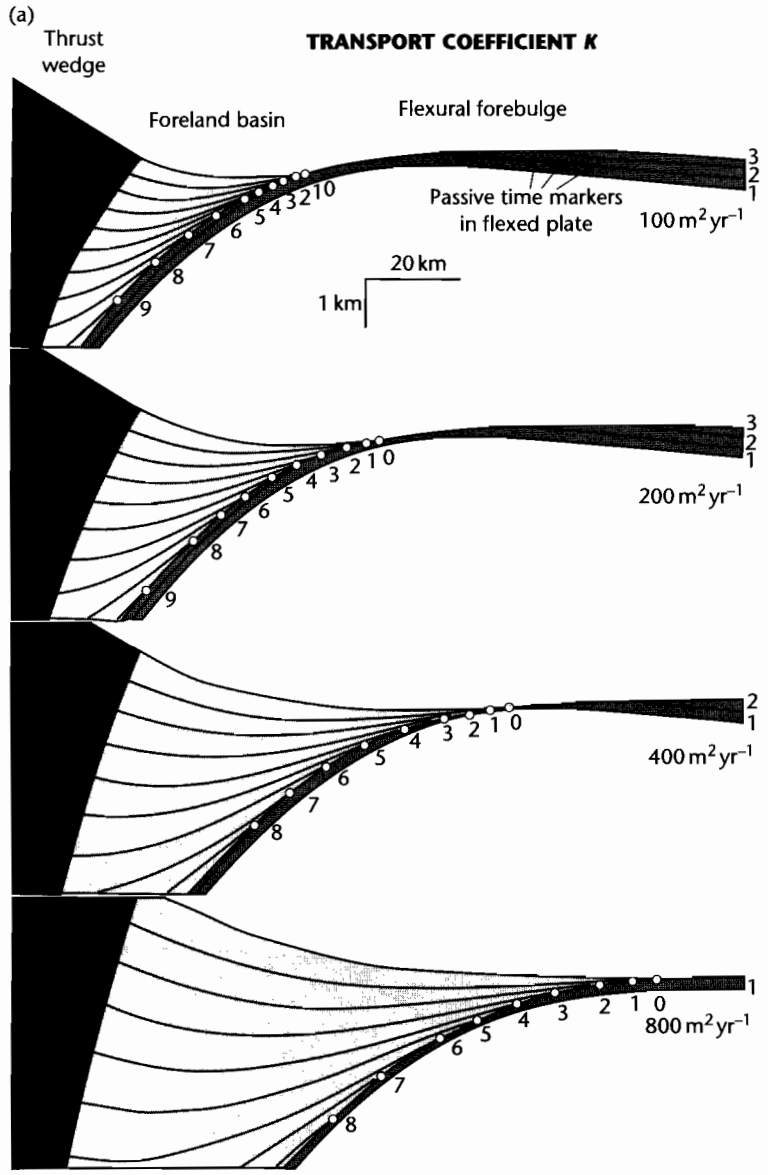

Fig. 4.33 Sensitivity tests of the parameters in Sinclair et al.'s (1991) diffusion model for mountain belt denudation and foreland basin evolution. The reference model involves a transport coefficient $K = 400\,m^2\,yr^{-1}$, slope angle = 1.5°, advance rate = $2.5\,mm\,yr^{-1}$, and equivalent elastic thickness of 20 km. In the sensitivity tests, one parameter is varied while the others are held constant at their reference values. Lines in basin are at equal time steps (chrons). Numbered positions on top of foreland plate are pinch-out (stratigraphic onlap) positions. Lines within foreland plate are passive markers to show extent of erosion of foreland plate in flexural forebulge. (a) Effect of variations in transport coefficient K, showing major impact on basin depth, basin width, and pinch-out migration rate; (b) Effect of variations in slope angle, showing major impact on basin depth, since sediment flux scales on slope; (c) Effect of variations in orogenic advance rate, showing major impact on pinch out migration rate; (d) Effect of variations in equivalent elastic thickness. Marine, underfilled basins are favored by low transport coefficients, low tapers, and fast advance rates, whereas continental overfilled basins are favored by high transport coefficients, high tapers, and slow advance rates, irrespective of flexural rigidity.

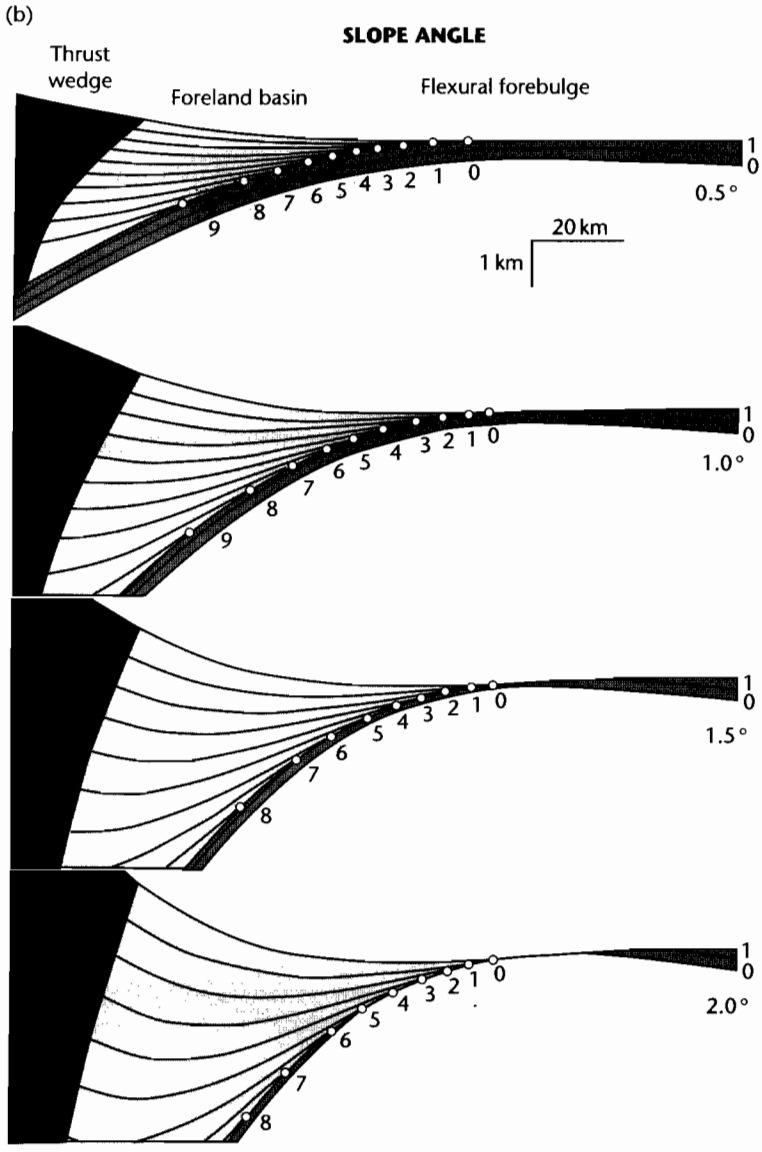

Fig. 4.33 *Continued*

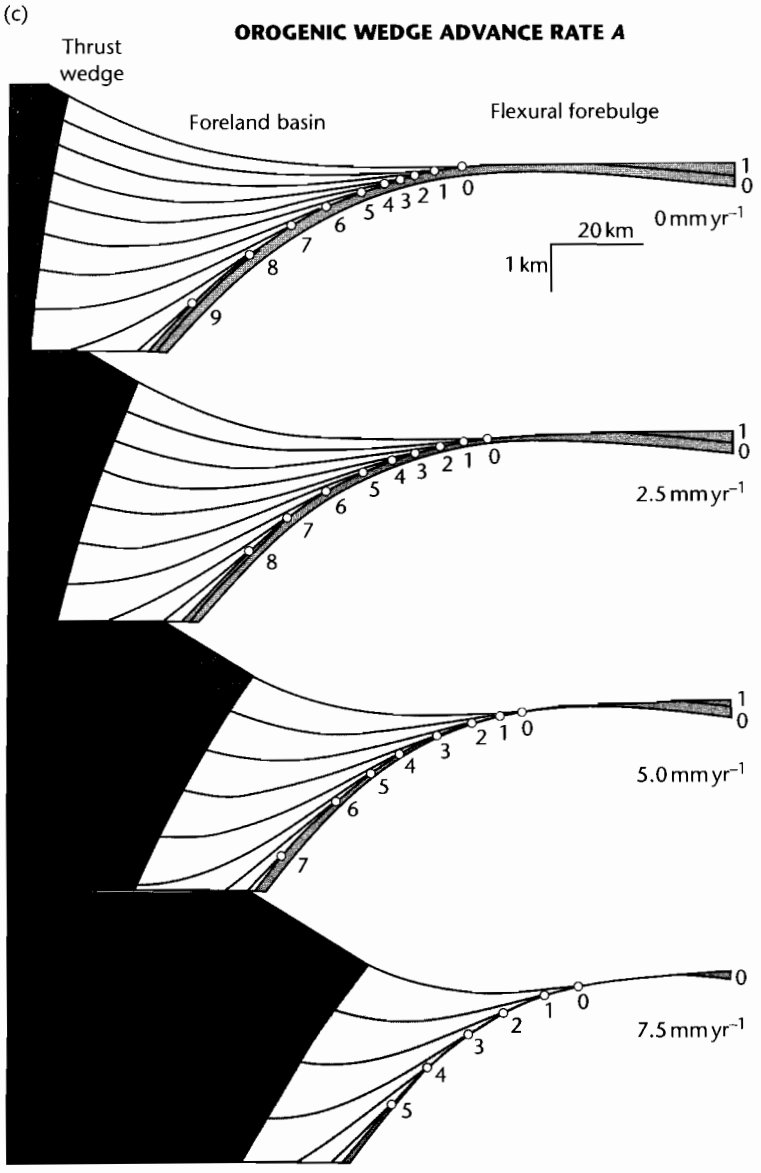

Fig. 4.33 *Continued*

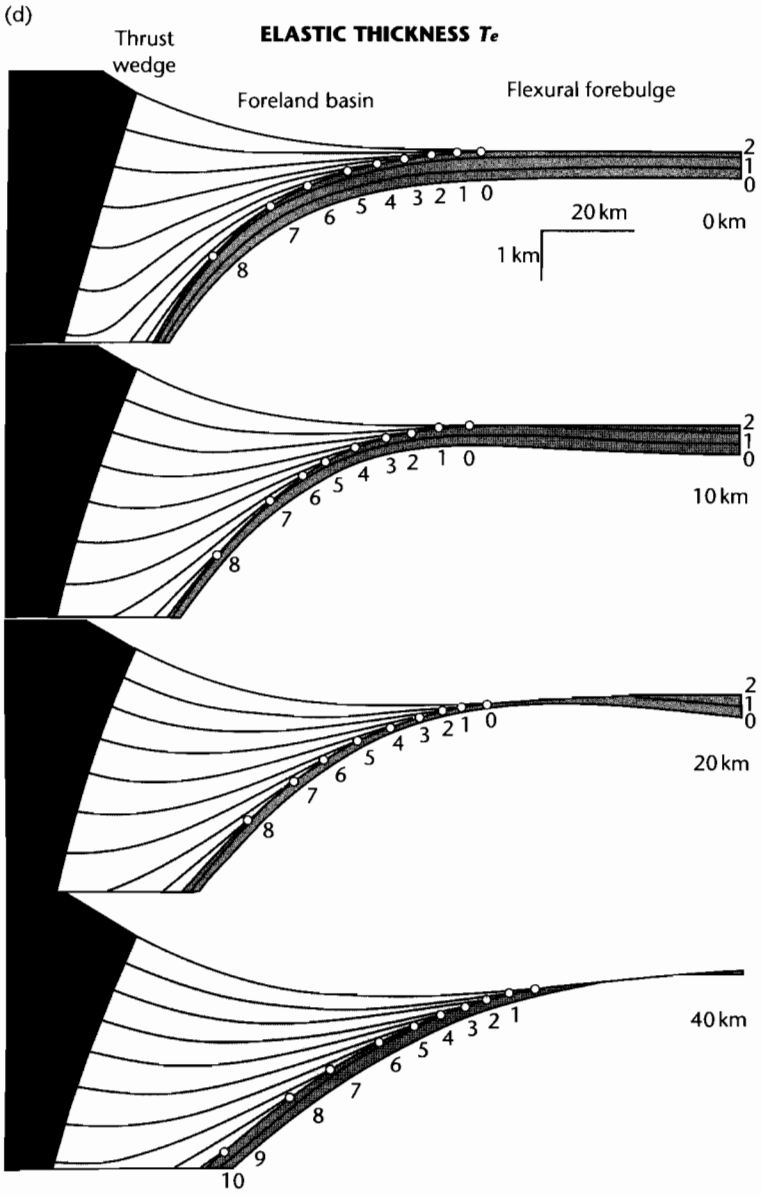

Fig. 4.33 *Continued*

ties in the North Alpine foreland basin of Switzerland, without the need to invoke viscoelastic relaxation of the lithosphere.

The effects of episodic thrusting have specifically been investigated (Flemings and Jordan 1989, 1990) using a model of a mountain belt as a fault-bend fold over a crustal scale ramp (Suppe 1983). Different transport coefficients were used for transport processes in rivers erosively incising the mountain belt and for alluvial rivers in the foreland basin. The change from quiescence to renewed thrusting was accompanied by a trapping of coarse sediment near the thrust front and the movement basinwards of the forebulge. Continued thrusting and sediment delivery to the basin forced the forebulge away from the orogen, causing stratigraphic onlap over an erosional unconformity. Other studies (Heller et al. 1988) suggest that during periods of tectonic activity, coarse clastic sediment wedges are trapped close to the thrust front, whereas during quiescence sediment is spread further from the thrust front, onlapping the basin margin (further discussion in §8.3). These different model results emphasize the importance of the fine detail of the different numerical models. Nevertheless, diffusional models have been helpful in enabling a link to be made between orogenic events and large-scale basin evolution.

4.6.3 Coupled tectonic-erosion dynamic models of bivergent wedges

Although a coupling between mountain belt denudation, exhumation, flexure, and deposition was made in the diffusional models discussed in §4.6.2, the coupling was through the arbitrary choice of an effective transport coefficient. This transport coefficient encapsulates all of the different factors influencing erosion, deposition, and sediment transport. In addition, tectonic fluxes have been crudely approximated (e.g., fault-bend fold over a crustal scale ramp) or left unspecified by use of a critical taper model. More recent models therefore have focused on: (i) a better treatment of the physical aspects of hillslope erosion, channel incision, and far field sediment transport, (ii) an investigation of the spatial variability of sediment routing systems and specifically the distribution of sediment entry points into the basin, and (iii) a coupling of realistic orogenic tectonic fluxes with exhumation patterns.

An early attempt to consider the mountain belt in planform and to incorporate the important geomorphic elements (hillslopes, channels) in the sediment routing system was the study by Koons (1989) of the Southern Alps of New Zealand. However, the channels were fixed and did not interact with the diffusive hillslopes in this early model. Subsequent models have incorporated the dynamics of stream incision, hillslope erosion, and sediment transport (see Chapter 7) on a deforming crustal template. A commonly used example at the orogenic scale is a 2-D plane strain thermomechanical model with a crust of thickness h with a strength profile determined by a brittle Coulomb-type upper layer and a temperature-dependent power-law lower layer (Willett 1992; Willett et al. 1993; Fullsack 1995). Below the crust are two mantle plates – one representing the subducting foreland lithosphere, and the other representing the overriding upper plate. Convergence between the two plates induces a shear force or traction on the base of the crustal layer, driving deformation. We have previously considered this type of model in terms of Argand number and Ampferer number (§4.5.4).

The tectonic development of the orogenic wedge, its isostatic compensation and its erosional unroofing, are clearly crucial to the analysis of foreland basins. On the basis of plane strain numerical models, we can consider the tectonic evolution of a convergent boundary such as the Alps of Europe as following three stages (Fig. 4.34) (Beaumont et al. 1996a):

1 Initially, tectonics are dominated by subduction of the pro-lithosphere due to the negative buoyancy of the downgoing slab (slab–pull effect). Subduction complexes form along a relatively thin shear zone above the subducting oceanic crust. Horizontal propagation of the accretionary prism is likely to be rapid, but the pro-foreland basin is likely to be underfilled with turbiditic "flysch."
2 In an intermediate stage, the subduction–collision transition, the subduction load decreases by the subduction of more buoyant continental lithosphere (or because of slab break-off), causing the pro-lithosphere to flexurally rebound. Parts of the pro-lithosphere detach and form part of a bivergent wedge instead of being subducted. Activity of a retro-shear should begin when the pro-lithosphere is no longer fully subducted during this transition phase.
3 In a final collision stage, when there is a negligible subduction load, well-defined pro- and retro-wedges form. The entire crustal pro-layer is incorporated into a critically tapered orogenic wedge. Denudation of the bivergent wedge should be particularly strong during this phase. Flexural basins (pro- and retro-

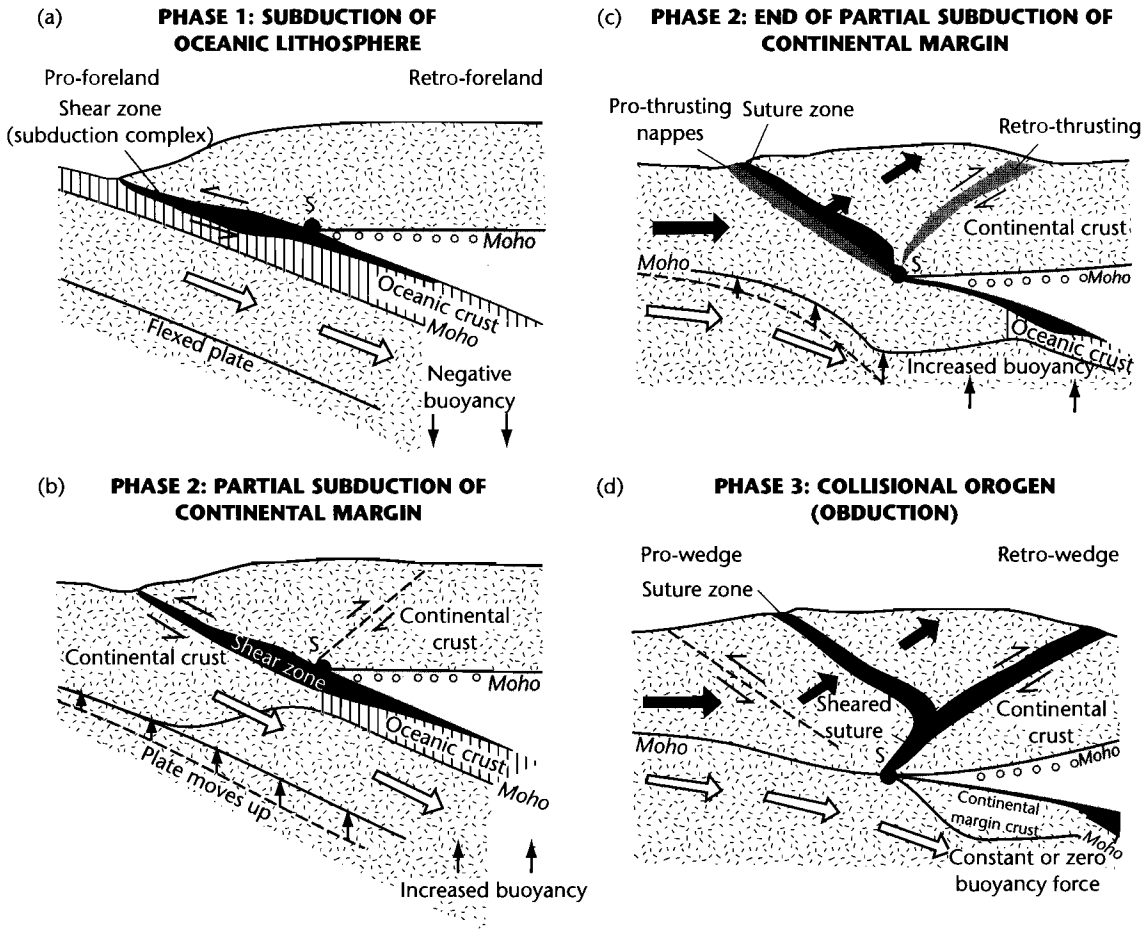

Fig. 4.34 Three-phase evolution of Beaumont et al.'s (1996a) plane strain finite element model from the subduction phase (phase 1) to the collision phase (phase 3). During phase 1 (a), the negative buoyancy of the lower plate is sufficient to fully subduct the entire plate. During phase 2 (b) and (c), the subduction load decreases because of continental lithosphere entering the subduction zone (and/or because of slab break-off). Progressively more of the lower plate detaches and a bivergent wedge begins to form. In phase 3 (d), all of the lower plate detaches to form a pro-wedge and continued propagation of deformation into the upper plate causes a retro-wedge to form. Convergence of pro-lithosphere with respect to stationary retro-lithosphere is shown by the white arrows. Black arrows show main transport direction of material in the pro-crust and wedge. Reproduced courtesy Geological Society of America.

foreland basins) are supplied with large amounts of basins, causing filling and overfilling in the "molasse" phase.

Since the tendency for thickened crust to spread laterally is strongly affected by the gravitational force, denudation of the orogen will hinder lateral tectonic progradation. If the rate of crustal thickening equals the rate of denudation, the orogen should not grow in size. We can refer to this as a *steady-state orogen*. The same idea applies to critically tapered Coulomb wedges (§4.5.2). If the wedge taper is reduced, for example by erosion, the Argand number falls, preventing lateral tectonic progradation. Only after internal deformation of the wedge has restored gravitational forces to a threshold level can the wedge continue to prograde laterally.

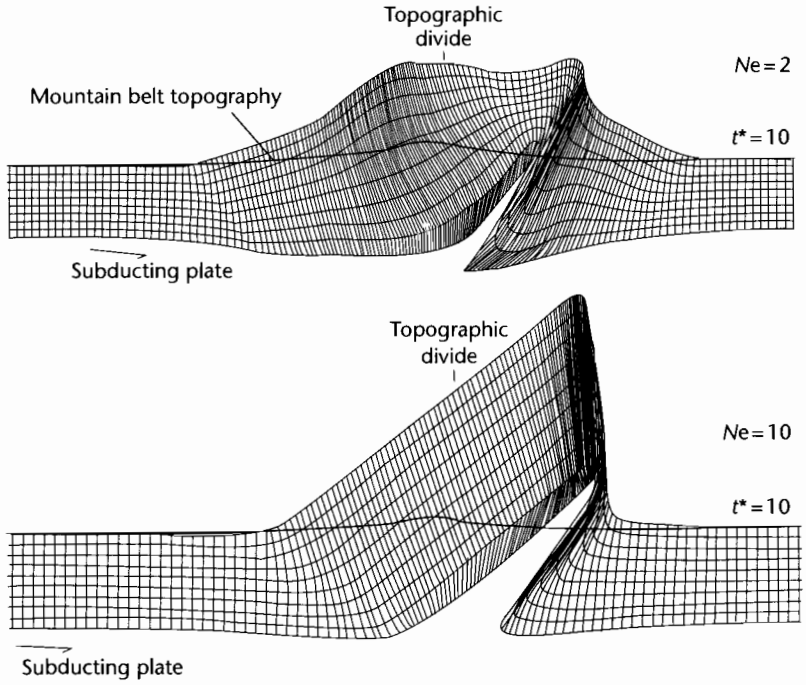

Fig. 4.35 Variations in coupled tectonic–erosion model for $Ne = 2$ and 10 for a dimensionless time of $t = 10$ ($t = tV_p/h$) (after Willett 1999). In both cases, elevation and exhumation have reached steady state. Note the greater amount of erosional removal of rock (exhumation) in the high erosion case. Reproduced courtesy of American Geophysical Union.

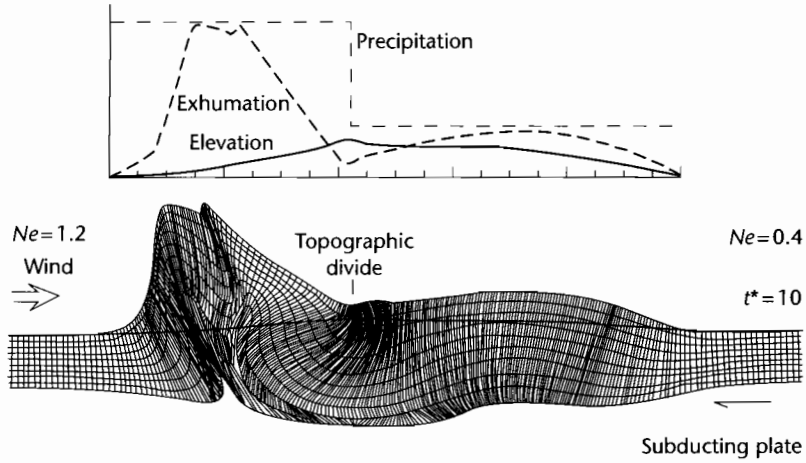

Fig. 4.36 Numcrical model of Willett (1999) with orographic focusing of precipitation such that the pro-wedge has an Erosion number Ne of 0.4 and the retro-wedge an Erosion number of 1.2, which closely reflects the precipitation patterns in the Southern Alps of New Zealand. Reproduced courtesy of American Geophysical Union.

Erosion at the surface can be modeled as either a function of elevation, relief or slope (Schlunegger and Willett 1999) or related to a set of geomorphic and climatic rules (Kooi and Beaumont 1994, 1996; Beaumont et al. 1996b; Willett 1999). As an example of the latter, erosion is commonly modeled through calculation of the rate of river incision, which is taken as proportional to stream power (Chapter 7). The efficiency of erosion versus tectonic uplift can be gauged from a dimensionless number, termed *Erosion number* by Willett (1999)

$$Ne = \frac{kL}{u} \tag{4.34}$$

where u is the rate of tectonic uplift, L is the half-width of the uplifting block of crust, and k is a coefficient proportional to the bedrock incision efficiency and precipitation rate with units time^{-1}. In the coupled tectonic-erosion model, Ne can be expressed in terms of the ratio between the accretion mass fluxes due to convergence (numerator) and the erosional mass flux through the upper surface (denominator), giving

$$Ne^* = \frac{4kL^2}{V_p h} \tag{4.35}$$

The Erosion number strongly controls the topographic profile and the exhumation pattern (Fig. 4.35). If Ne tends to infinity, erosion planes off the topography ruthlessly despite finite rates of tectonic uplift. The Erosion number Ne strongly controls the time taken for a mountain belt to achieve steady state and its maximum elevation. Coupled models therefore now allow specific precipitation patterns, such as wet orographic flanks (high Ne) and dry rain-shadow flanks (low Ne) to be investigated as mechanisms for particular patterns of exhumation and topography (Fig. 4.36).